2009

Study of circular and elliptical tube arrays as cross flow heat exchangers

Mohamed Abdulrahman M Mosa
University of Windsor

Study of Circular and Elliptical Tube Arrays as Cross Flow Heat Exchangers

by

Mohamed Abdulrahman M. Mosa

A Thesis
Submitted to the Faculty of Graduate Studies
through the Department of Mechanical, Automotive, and Materials Engineering
in Partial Fulfillment of the Requirements for
the Degree of Master of Applied Science at the
University of Windsor

Windsor, Ontario, Canada
2009

Your file Votre référence
ISBN: 978-0-494-57641-0
Our file Notre référence
ISBN: 978-0-494-57641-0

Author's Declaration of Originality

I hereby certify that I am the sole author of this thesis and that no part of this thesis has been published or submitted for publication.

I certify that, to the best of my knowledge, my thesis does not infringe upon anyone's copyright nor violate any proprietary rights and that any ideas, techniques, quotations, or any other material from the work of other people included in my thesis, published or otherwise, are fully acknowledged in accordance with the standard referencing practices. Furthermore, to the extent that I have included copyrighted material that surpasses the bounds of fair dealing within the meaning of the Canada Copyright Act, I certify that I have obtained a written permission from the copyright owner(s) to include such material(s) in my thesis and have included copies of such copyright clearances to my appendix.

I declare that this is a true copy of my thesis, including any final revisions, as approved by my thesis committee and the Graduate Studies office, and that this thesis has not been submitted for a higher degree to any other University or Institution.

ABSTRACT

Maximizing the heat transfer and reducing both the flow resistance and the overall size are vital in heat exchangers design. In view of that, in the present study circular and elliptical tubes were studied as the basic components of heat exchangers. The tubes were arranged to form single in line circular and elliptical tube arrays. The circular tube array consists of 10 tubes with diameter of 22.25 mm, while the elliptical tube array consists of 18 tubes with axis ratio of 0.3. In both arrays, 6.2 mm gab between each two adjacent tubes was kept. The experiments were conducted in a closed loop thermal wind tunnel facility with a 305 mm x 305 mm x 600 mm test section. The study was for heating of air via water in cross flow. For the two arrays, Re_a was ranged from 17000 to 49000, and m_w was varied from 0.01 to 0.11 kg/s.

The study revealed that mainly the Reynolds number controls the heat transfer mechanism at the air side. Correlations in term of Nu_a and St_a variations with Re_a were established. Also, the pressure drop across the arrays was observed and the results were correlated in term of P_{dc} as a function of Re_a. The results concluded that enhancement in the heat transfer of 70 % and reductions in the pressure drop of 79 % were achieved by utilizing the elliptical tubes as relative to the circular tubes. For the water flow, the variation of Nu_w with Re_w was observed. An overall combined correlation applicable for the water flow inside the circular and elliptical tube arrays was established.

To my family

ACKNOWLEDGEMENTS

I wish to acknowledge the various individuals and organizations who contributed to this research. First of all, I wish to express my sincere gratitude to my thesis adviser Dr. Amir Fartaj for his supervision throughout the duration of my Master's program. This work would likely not have accomplished without his guidance, insight and the very friendly environment he provided. I also wish to deeply thank Dr. Faouzi Ghrib and Dr Henry Hu, who accepted to be in my thesis committee.

I am very grateful to the Libyan Scholarship Program for the financial support administrated through the Libyan cultural Section in Canada. I am also thankful to the Department of Mechanical Engineering for GA opportunity, technical support provided through Mr. Andrew Jenner and Mr. Patrick Seguin, and the secretarial services of Ms. R. Gignac.

I am also thankful to my colleagues who were of great support for the duration of my study. A special thank goes to my lab partner Mesbah with whom I had the opportunity work and discuss my research. I would also like to deeply thank my colleague Ghassan for his help and encouragements from the first day we met.

My sincere gratitude goes to my family members. Special thanks to my beloved parents for their unending love and support. Last but not least, my thanks are due to all my Libyan friends in Windsor and in my home city, Tobruk.

TABLE OF CONTENTS

LIST OF TABLES

LIST OF FIGURES

NOMENCLATURE

a	Semi-major axis length of the elliptic tube [m]
2a	Major axis length of the elliptic tube [m]
A	Cross-sectional area [m^2]
A_s	Surface area [m^2]
AR	Axis ratio
B	Bias Error
b	Semi-major axis length of the elliptic tube [m]
2b	Minor axis length of the elliptic tube [m]
c_p	Specific heat [KJ/Kg. ^{o}C]
D	Circular tube diameter [m]
D_h	Hydraulic diameter [m]
FR	Flow rate [m^3/s]
f	Friction factor
g	Gravitational acceleration [m/s^2]
Gr	Grashof number
h	Convection heat transfer coefficient [W/ m^2.^{o}C]
k	Thermal conductivity [W/ m.^{o}C]
L	Tube length [m]
m	Mass flow rate [kg/s]
Nu	Nusselt number
P	Perimeter [m] or Precision Error
P_{dc}	Air side pressure drop coefficient
P_{dyn}	Dynamic pressure [Pa]
Pr	Prandtl number
P_{static}	Static pressure [Pa]
P_{total}	Total pressure [Pa]

Q	Heat transfer rate [Watt]
Re	Reynolds number
S	Tube to tube spacing [m]
S_{dm}	Standard deviation of the mean
S_t	Stanton number
T	Temperature [°C]
V	Reference velocity [m/s]
$V_{a\ max}$	Velocity at minimum cross-sectional area [m/s]
Z	Characteristic length [m]

Greek Symbol

ΔP_a	The pressure drop of the air across the tube array [Pa]
α	Thermal diffusivity [m^2/s]
β	Coefficient of thermal expansion [K^{-1}]
μ	Dynamic viscosity [Kg/m.s]
ν	Kinematic Viscosity [m/s^2]
ρ	Density [Kg/m^3]

Subscripts

a	Air
b	Bulk
e	Exit
f	Film
h	Hydraulic
i	Inlet and Inner
max	Maximum
o	Outer
s	Surface
t	Total
w	Water

CHAPTER 1
INTRODUCTION

Heat transfer from one hot fluid to another cold one usually takes place in a device called heat exchanger. Heat exchangers are encountered in many industrial applications. They are found in oil industries, power plants, heating and air conditioning systems etc. Such devices can be categorized based upon application, flow arrangement, type of the working fluids etc. Cross flow heat exchangers in particular, which are classified under the flow arrangement category, are widely used in practical applications. In this kind of heat exchangers, a typical way that heat exchange occurs between two unmixed heat transfer carriers flowing perpendicular to one another. Heat transfer process in such equipment is driven mainly by forced convection. A car radiator is a common example of this type, where the engine coolant is pumped inside the radiator tubes and dissipates heat to the air sucked by a fan to flow over the exterior surface of the tubes.

Cylinders of various shapes are commonly employed in cross flow heat exchangers. A wide range of extensive studies have been carried out concerning heat transfer mechanism and flow structure over such objects in cross flow. The continuous objective behind these investigations is maximizing heat transfer rate and minimizing pressure drop across heat exchangers. In this regard, numerous numbers of experimental and numerical investigations have been carried out on a row of a single tube, a single row of tubes, and tube banks in cross flow. As heat transfer augmentation and pressure drop decreasing considered, many new techniques and procedures introduced to serve this matter and provide clear picture of the parameters involved. Examples of these techniques are: changing tubes arrangement, introducing fins on the surfaces of the tubes to increase heat transfer area, using different tube shapes etc. In general, enhancement of heat transfer rate in heat exchangers is more required in gases side than liquids side. This is due to the higher thermal resistance of gases. According to Khan et al. (2005), Wang (2000) indicated that for heat transfer between air and water in cross flow, the airside usually accounts for up to 90% of the total thermal resistance.

A review of the literature has shown that heat transfer rate and pressure drop in cross flow heat exchangers depend upon many factors. Several studies have indicated that parameters such as Reynolds number, Re, thermo-physical properties of fluids, tubes materials, and their arrangement have significant influence on thermal and hydraulic performance of heat exchangers. The effects of such parameters on heat transfer rate and pressure gradient in cross flow heat exchangers with various cross sections (circular, elliptical, rectangular etc) have been the focus of many investigations. The flow over circular tubes in particular has been extensively studied during the past decades.

In recent years, tubes with elliptical cross sections have received much attention. Results from several studies have revealed that elliptical cylinders have many advantages over circular ones in term of thermal and hydraulic performance. Many studies have shown that the resistance of the flow over an elliptical cylinder is less than that of a circular cylinder of the same perimeter, resulting in a less power requirement to drive the flow. Furthermore, heat transfer area in a given volume for an elliptical cylinder is larger than that of a circular one, which is more beneficial, when a gas such air is used as heat transfer medium. In the current study, the heat transfer characteristics of inline circular and elliptical tube arrays placed in cross flow are experimentally investigated by using air and water as standard heat transfer media.

1.1 Motivation

With the ongoing development in the modern industry, an urgent objective of developing thermal system devices that occupy the smallest possible space and provide high efficient performance is required. Thus, designing heat exchangers to provide minimum thermal and flow resistances and save application space is of primary interest. In view of that, circular and elliptical cylinders are used as the basic heat exchangers components in this study. The following considerations were the motivations to conduct the present research:

- Review of the earlier work has shown that most of the previous work has been focused on circular tubes as a typical geometry for heat transfer characteristics and flow structures study. Limited work has been given to elliptical tubes, especially for the case of a single inline tube array.
- A single elliptical tube provides larger heat transfer area as relative to a circular tube which increases heat transfer rate.
- An elliptical tube occupies smaller space than a circular one, which results in reduction in the overall size of the application.
- A body of an elliptical cylinder offers less resistance to the flow than that of a circular one. Therefore, less pressure drop is encountered, and thus, less power is required to circulate the flow.

1.2 Objective

The primary objective of the present research is to investigate the air flow heat transfer and the pressure drop features of inline circular and elliptical arrays of tubes. In addition to that, the water flow heat transfer performance is investigated. This has been conducted as follows

- Airside heat transfer coefficient to be obtained in the dimensionless form of Nusslet number, Nu_a, and Stanton numbers, St_a. Correlations of Nusslet and Stanton numbers with Reynolds number, Re_a, to be established.
- Air flow pressure drop features across the arrays to be examined and presented in dimensionless form as a function of Reynolds number.
- Water flow heat transfer coefficient in the dimensionless form of Nusselt number to be obtained and correlated with Reynolds number.
- Results to be compared with others from the available literature.

CHAPTER 2
LITERATURE REVIEW

Due to the importance of heat exchangers in many engineering applications, a wide range of extensive studies have been carried out to optimize the performance of such devices. A review of the available literature has shown that the thermal and hydraulic performance of heat exchangers relay upon many parameters. Such parameters include: tube shape, arrangement of tubes, orientations of tubes etc. The below is a brief review of some of the previous work considering cylinders as the basic components of heat exchangers in cross flow.

2.1 Circular and Elliptical Tubes in Comparison

Comparisons of circular and elliptical tubes as the essential elements of heat exchangers have been reported in several studies. For example, Brauer (1964) reported 18 % of relative reduction in the pressure drop comparing elliptic and circular tubes arrangements. Matos et al. (2001) used the finite element method to study the heat transfer characteristics for circular and elliptical tubes heat exchangers in cross flow of air. The tubes were arranged in a staggered configuration. Reynolds number based on the array length was in the range of 300 to 800. Their results revealed that a relative gain of 13% in heat transfer and up to 25% reduction in pressure loss is obtained in the case of the elliptical tube. The results were reported for circular and elliptical tubes with the same obstruction area to the flow. Khan et al. (2005) reported that Sohal and O'Brien (2001) found that an elliptical tube with axis ratio of 0.33 having the same cross sectional area as of a circular can enhance the heat transfer by 25 to 35 %. Another study was that conducted by Horvat et al. (2006). They numerically investigated the transient heat transfer and fluid flow for circular, elliptical, and wing shaped tubes with the same cross section. Reynolds number based on the averaged time velocity and the hydraulic diameter was varied to cover the three flow regimes (laminar, transitional, and turbulent regimes). The investigation was for tube-to-tube spacing to diameter ratio of 1.125 to 2. As a comparison between the three types of tubes, they reported that the drag coefficient for the elliptical and the wing shaped tubes is lower than that of the circular tube. Mainardes et al. (2007) experimentally studied the forced convection of circular and elliptical finned tube with the same obstruction area to the flow placed in cross flow. The investigation was performed for air Reynolds number (with the minor axis as the characteristic length) range of 2650 to 10600 with tube spacing to minor diameter ratio was varied from 0.1 to 1.5. The results reported a gain of up to 80% in heat transfer is achieved when using the elliptical tubes compared to the circular ones.

2.2 Role of the Axis Ratio of the Tube

The axis ratio as defined by Badr (1998) is the ratio of the minor axis to the major axis of a tube. Other definitions found in the literature for the axis ratio include the aspect ratio as referred to by Oliver and Rao (1979), tube flatness as of the definition introduced by Harris and Goldschmidt (2002), or eccentricity as mentioned by Mainardes et al. (2007). The influence of this parameter on heat transfer has been reported in many studies. For example, Badr (1998) in his study of forced convection from an elliptical tube located in cross flow of air examined the effect of the axis ratio on heat transfer. The investigation included four axis ratios, 0.4, 0.5, 0.7, and 0.9. For Reynolds number in the range of 200 to 500, the results showed that the 0.4 axis ratio provided the highest heat transfer rate. In the numerical study conducted by Matos et al. (2001), it was concluded that for axes ratios in the range of 0.6 to 1 as the axis ratio decreases as the heat transfer rate increases. Harris and Goldschmidt (2002) experimentally studied the overall heat transfer coefficient between a fuel flowing in an elliptical cylinder and the air passing over the cylinder in cross flow. The study covered three-axis ratio, 0.2, 0.31, and 0.52). For Reynolds number from 2300 to 6700 with the major axis parallel to the flow direction, their results showed that the axis ratio of 0.2 provided the highest overall heat transfer coefficient.

2.3 Role of Tube Spacing

Tube spacing is an important factor that influences heat transfer and pressure drop features of flow a single row of tubes or bundle of tubes. The effect of this parameter has been observed in several studies. Nishiyama et al. (1988) conducted an experimental study of flow pattern and heat transfer characteristics around four cylinders of elliptical cross section. The cylinders have a major axis of 50 mm and a minor to major axis ratio of 0.5. Considering the major axis as the characteristic length, Reynolds number was varied from 15000 to 70000. The cylinders spacing in the dimensionless form of center-to-center distance and major axis ratio was ranged from 1.25 to 4. The results indicated that to achieve high heat transfer coefficient, the cylinders are to be spaced as close to each other as possible. Wilson et al. (2000) theoretically studied heat transfer and pressure drop characteristics of single row of tubes in cross flow of air. The Reynolds number ranged from 500 to 100000. They examined the tube spacing effect in the form of traverse- spacing to diameter ratio. This spacing ratio was varied from 1.3 to 5. They revealed that the maximum heat transfer coefficient and the minimum pressure loss are obtained at small traverse-spacing to diameter ratio.

2.4 Role of Angle of Attack

The flow angle of attack is another parameter that affects heat transfer performance of flow over cylinders. This angle is defined as the angle between the free stream direction and the front stagnation point of a tube. The influence of such factor on the heat transfer coefficient has been reported in a number of studies. Nishiyama et al. (1988) concluded that for angles of attack in the range of 0^{o} to 90^{o}, the maximum heat transfer rate is obtained at 0^{o} angel of attack. Badr (1998) used a numerical approach to investigate the forced convection from an elliptical tube situated in cross flow with air as working fluid. Ranging Reynolds number from 20 to 500 and the angle of attack from 0^{o} to 90^{o}, his results showed that the maximum heat transfer coefficient is reached at 0^{o} flow angle of attack and minimum heat transfer occurred at 90^{o}. Nada et al. (2007) conducted an experimental and numerical study to investigate the heat transfer and flow characteristics over a tube of a semi-circular cross section positioned at different angles in cross flow. Reynolds number based on the tube diameter was ranged from 2200 to 45000. Their findings indicated that orienting the tube with the arched surface normal to the flow direction (zero angle of attack) provided the maximum Nusselt number. Ibrahim and Gomma (2009) performed experimental and numerical studies of the turbulent flow in bundle of elliptic tubes. The investigation cover Reynolds number range from 5600 to 40000. Four axis ratios considered, 0.25, 0.33, 0.5 and 1, and flow angle of attack was varied from 0^{o} to150^{o}. Their results show that, the maximum thermal performance under a fixed pumping power is obtained 0^{o} flow angle of attack and the minimum thermal performance was obtained at an angle of attack of 90^{o}.

2.5 Scope of the Current Research

In view of the previous work, single circular and elliptical arrays of tubes arranged in inline configuration were experimentally studied as cross flow heat exchangers. 10 circular tubes and 18 and elliptical tubes were situated in a 305 mm x 305 mm x 600 mm test section to form two inline tube arrays.. The tubes were oriented at zero flow angle of attack with 6.2 mm gab between each two adjacent tubes. Each elliptical tube was formed from a single circular tube having the same dimensions as in the circular tube array. The elliptical tubes manufacture to provide axis ratio of 0.3 with miner and major axis lengths of 9.7 mm and 31.7 mm, respectively. The elliptical tubes were situated in the array with the major axis parallel to the flow direction. The tube arrays were tested for heating of air via water in cross flow under similar operating conditions. The air flow Reynolds number was varied from 17000 to 49000 to cover a wide range applicable for heat exchangers applications.

CHAPTER 3

EXPERIMENTAL SETUP AND PROCEDURE

3.1 Experimental Setup

This research was carried out in the Thermal Management laboratory located in the Engineering Building at the University of Windsor. The experimental setup consists of a closed loop thermal wind tunnel, a water supply system, two single tube arrays heat exchangers, data acquisition system and measurement instrumentations. Figure 3.1 below shows a schematic of the experimental setup and details of the test facilities are provided in the following sections.

3.1.1 Thermal Wind Tunnel

A closed loop thermal wind tunnel of 5440 mm length, 750 mm width, and 1640 mm height was used to carry out this study. A hydraulic pump was used to drive a blower to force the air to circulate through the wind tunnel duct. A variable speed electrical motor was used to power the pump to produce the required air velocities. In the absence of any obstruction in the flow direction, the wind tunnel is capable of producing a maximum velocity of 30 m/s. The wind tunnel has a 305 mm x 305 mm x 600 mm test section. An auxiliary tubular heat exchanger installed in the tunnel duct at the upstream side of the air passage to provide control over the air temperature at the inlet.

1 Variable speed motor
2 Hydraulic pump
3 Blower
4 Heat exchanger
5 Water supply lines
6 Static Pitot tube
7 Pressure transducer for velocity measurement
8 Water inlet temperature measurement
9 Water flow meter
10 filter
11 Water inlet pressure measurement
12 Pressure drop across heat exchanger measurement
13 Water exit temperature measurement
14 Water exit pressure measurement
15 Test section
16 Data acquisition system
17 Computer

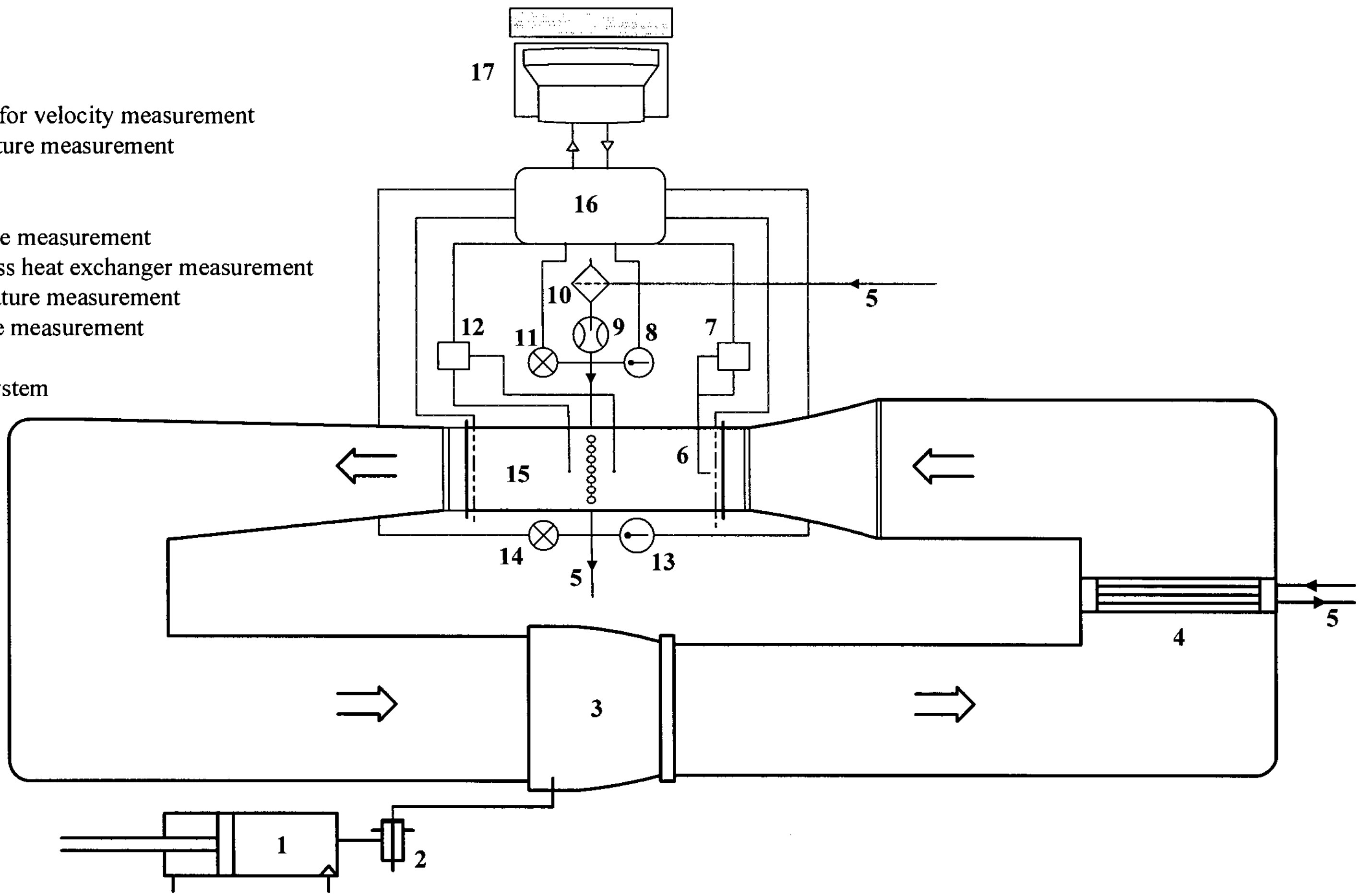

Figure 3.1 A schematic of the experimental setup

3.1.2 Circular Tube Array Heat Exchanger

Figure 3.2.A below displays a schematic of the test section with the circular tube array. The test section is a square duct of 305 mm wide, 305 mm high and 600 mm long made of Plexiglas with thermal conductivity 0.19 W/m.°C. 10 circular tubes made of copper with thermal conductivity of 339 W/m. °C were arranged to form an inline single row of tubes situated horizontally in the middle of the test section. Each tube has an outside diameter of 22.25 mm and wall thickness of 0.825 mm. The tubes are arranged by 6.2 mm gap between each two adjacent tubes and placed at zero flow angle of attack. Two half tubes, dummy, were added at the bottom and top of the array to maintain the space of 6.2 mm between each two adjacent tubes.

3.1.3 Elliptical Tube Array Heat Exchanger

In order to make a comparison with the circular tube array, another test section with the same dimensions and materials was manufactured and instrumented with 18 elliptical tubes with minor to major axis ratio of 0.3 forming a single array of tubes as shown in figure 3.2.B. The array positioned at the middle of the duct with the tube minor axis perpendicular to the flow direction at zero flow angle of attack. The traverse distance between the outer surfaces of any two neighbouring tubes was keep at 6.2 mm as in the other array. Two half dummy tubes connected to the duct walls were also introduced to keep the 6.2 mm space between the tubes. Each elliptical tube was formed from a 22.25 mm diameter 0.825 mm thickness circular tube to give the same surface area as any circular tube in the other array.

Figure 3.2.A Circular tube array

Figure 3.2.B Elliptical tube array

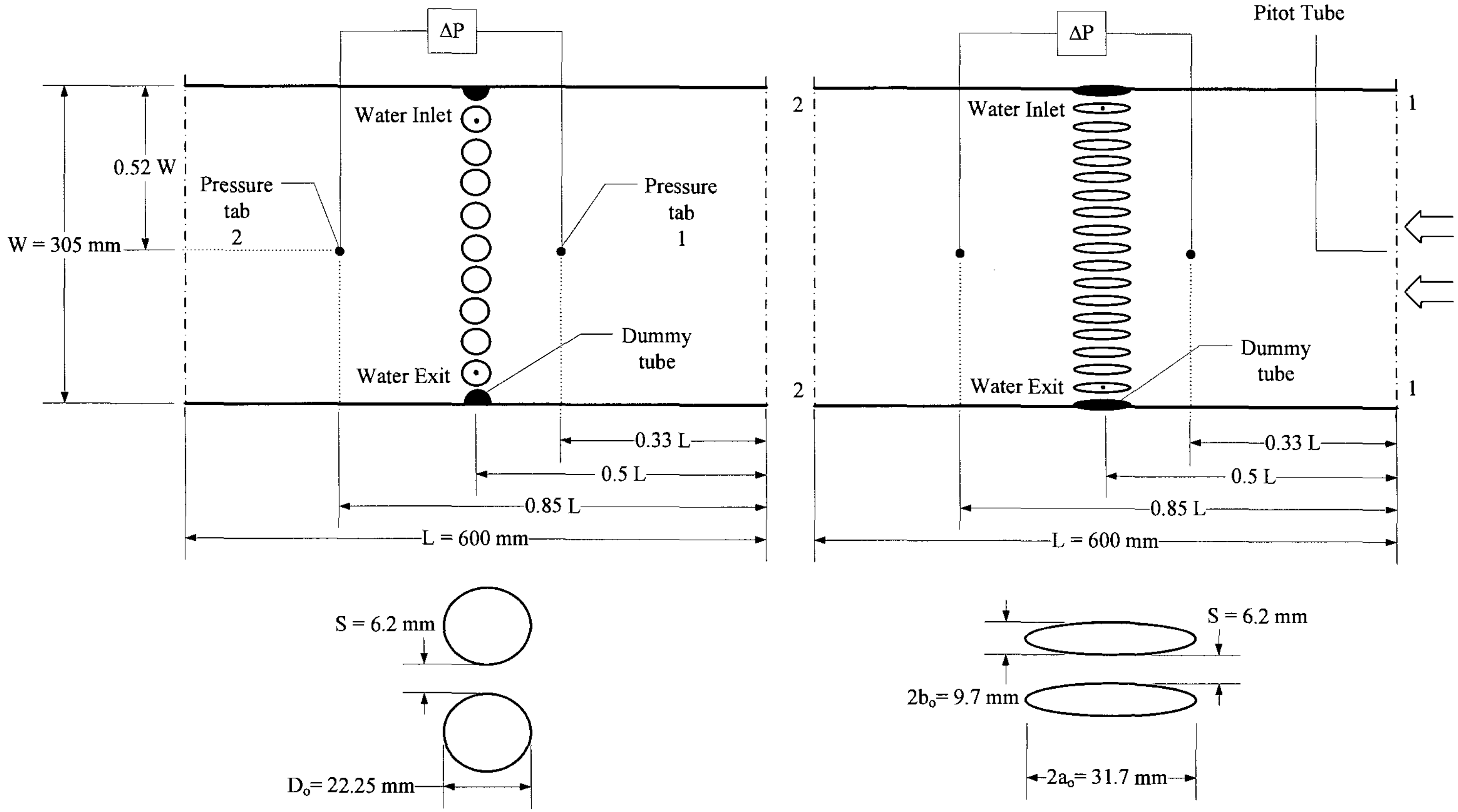

Figure 3.2 Schematics of the test section with the circular and elliptical tube arrays

3.1.4 Data Acquisition System

Signals from the air and water flow measurement devices were fed to data acquisition provided by National Instruments and monitored via LabView software. The data acquisition consists of I/O board, NI-PCI-6052E, three thermocouples signal conditioning modules, SCXI-1102, and three isothermal terminal blocks, SXCI- 1303. The SCXI-1303 is designed for high accuracy temperature measurement. It has 32 input channels to provide signal to SCXI-1102 module. The data acquisition system provides flexibility and control over the number of instrumentations to be used. It allows additional measurement devices to be added (or removed) as necessary. The modules can be placed close to the experimental measurement location which helps reduce any unnecessary cable length. In the current study the total number of channels was 96 (3 modules x 32 channel). 84 channels were allocated for thermocouples measurements and 12 for analog input data (pressures, air flow velocity, water flow rate etc.). Data were collected and monitored through a computer.

3.1.5 Water Supply System

Cold and hot water lines were supplied to the experimental setup from the main line designed for laboratory use. The system is designed to supply water to the tube arrays and the heat exchanger installed inside the duct of the wind tunnel. In the current study, cold water line was drawn to directly feed the heat exchanger in the wind tunnel duct. Another hot water line was delivered to the tube arrays. In this case, the air flow inlet temperature was always less than that of the water. When necessary both lines were mixed together in a mixing chamber and fed to the proper location.

3.2 Experimental Procedure and Operating Conditions

Study of heat transfer mechanism between air flowing over circular and elliptical tube arrays and water passing inside the tubes, was the main objective of this study. This was conducted by heating of air via hot water in cross flow. Air was forced to flow over two arrays of tubes, circular and elliptical, and exchange heat with the water flowing in the inside part of the tube. The same thermal and flow conditions were applied on both tube arrays. The air and water inlet temperature were maintained constant. The air flow inlet temperature was kept at 18 ± 2.5 °C, while for the water flow inlet temperature was in the fixed 35 ± 2.5 °C. The air velocity was manually controlled by adjusting a valve connected to the electric motor driving the hydraulic pump to reach desired conditions. The water flow rate was also manually set to a certain value and then supplied to the experimental side. In the circular tube case, six air flow velocities ranging from 2.6 to 7.4 m/s corresponding to six Reynolds number (based in the tube outer diameter) in the range of 17000 to 49000 were varied with different water flow rate varying from 0.01 to 0.11 kg/s. For the elliptical tube array, the air velocity was varied with the same water flow rate range as in the circular tube from 3.3 to 9.5 m/s to give based on the tube major axis six the same Reynolds number range as in the other array, 17000 to 49400. In order to account for any fluctuation in the air and water inlet conditions, adequate time, 40 to 50 minutes, were allowed before any single test run to ensure that the system has stabilized.

3.3 Measurement and Experimental Data Collection

To establish a relationship between the air flow velocity and the heat transfer rate and the associated pressure drop under predetermined conditions, simultaneous measurements of different experimental parameters were performed. Measurements parameters include, air velocity, water flow rate, air and water inlet and exit temperature, surface temperature, and pressure drop across the arrays. Below is description of the measurement for these parameters.

3.3.1 Temperatures Measurements

In this study, all temperatures were measured using thermocouples type T. Each single thermocouple was calibrated over the temperature range considered in this study. The calibration was performed using Dry Block Calibrator, CL-770A, provided by Omega. The device is capable of producing temperature range from 45 °C below ambient to 140 °C. The thermocouples probes were assigned to measure the temperature at specified locations and signal form each probe was sent to the data acquisition system board through the isothermal terminal block.

Air Inlet and Exit Temperature Measurements

Air flow inlet and exit average temperatures, T_{a_i} and T_{a_e}, were measured by thermocouple arranged in grids as shown in figure 3.4. For the inlet measurement, a grid of 9 thermocouples arranged uniformly across the inlet cross section was used. At the exit cross section, a grid consists of 16 points was used to estimate the average temperature at the exit.

Water Inlet and Exit Temperature Measurements

Water flow inlet and exit temperatures, T_{w_i} and T_{w_e}, were measured by mean of a single point measurement. One insert type thermocouple was installed at each location.

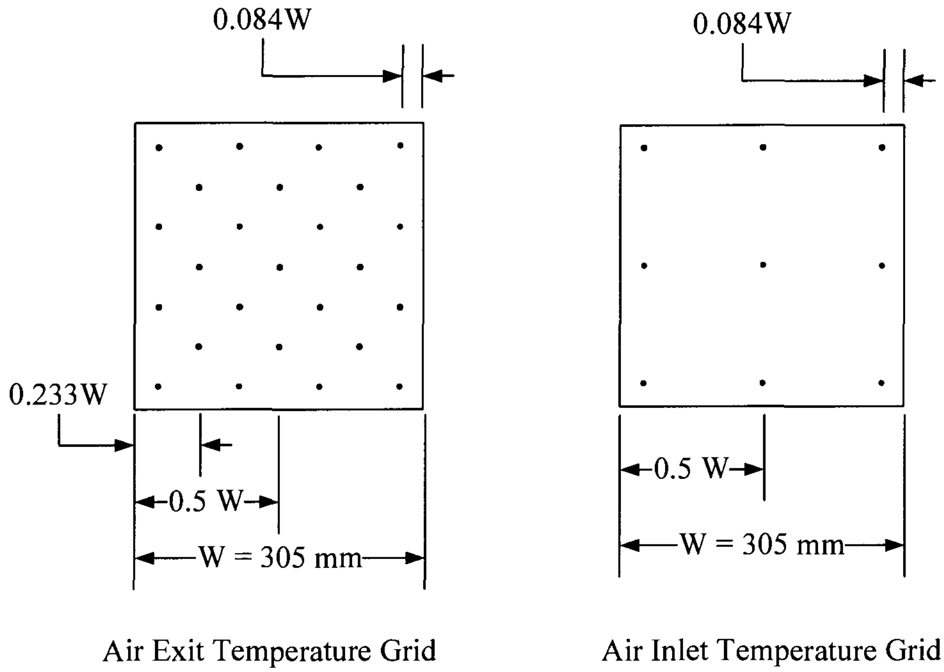

Figure 3.3 Air Inlet and Exit Temperature Grids

Tube Surface Temperature Measurements

The surface temperature of the tubes, T_s, was measured by attaching 3 thermocouple probes on the outer surface of each tube in the array. For the circular tube array consisting of 10 tubes, 30 thermocouples were fixed on the outer surface of the tubes. In the case of the elliptical tube array, 18 tubes, the total number of temperature probes were 54. The average temperature of single tube was taking to be the average of the three probes attached to its surface.

3.3.2 Measurements of the Upstream Air velocity, Absolute Pressure and Pressure Drop across the Arrays

Measurements of the Upstream Air velocity and the Absolute Pressure

The air velocity at the inlet, V_a, and the absolute pressure, P_{ab}, inside the test section were measured simultaneously using a Pitot static tube and pressure acquisition system provided by Flow Kinetics, FKT3PDA. As shown in figure 3.4 below, a pressure line drawn from the low pressure port of the Pitot tube was divided into two parts. One part was connected to an absolute pressure transducer to read the absolute pressure. The other one was connected along with the line drawn from the total pressure port to a differential pressure transducer to read the dynamic pressure, P_{dyn}. From the dynamic pressure the inlet air velocity was calculated based on Eq. (3.1).

$$V_a = C\sqrt{\frac{2\ P_{dyn}}{\rho_a}} \tag{3.1}$$

where *C* is a correction depends on the design of the Pitot Tube. For the Pitot tube used in the current study, C was equal to 1.

To determine the average air velocity at the inlet, a plane of 25 measurement points at the inlet cross section as shown in figure 3.5 was surveyed using the Pitot tube. The Pitot tube was traversing the square cross section area over each measurement location. The measurement points' locations were chosen in accordance with the ASHRAE standard using the Log-Tchebycheff method. In this method, the locations of traverse points are chosen to accounts for the effect of wall friction and the velocity drop near the test section wall.

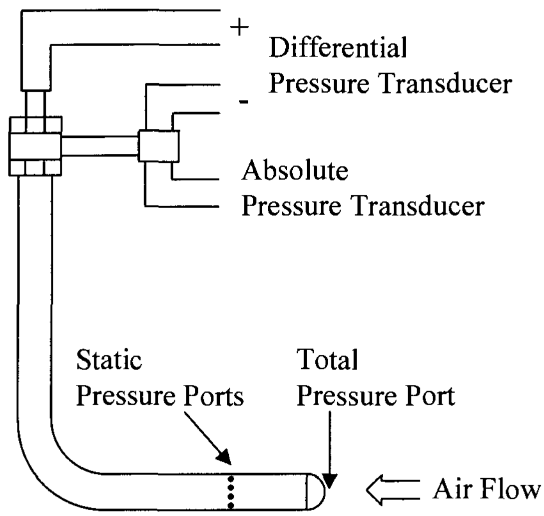

Figure 3.4 Pitot static tube

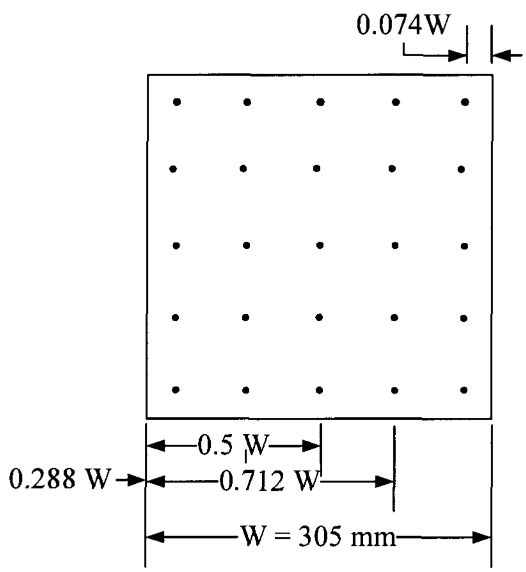

Figure 3.5 Velocity grid

Measurements of Air Pressure Drop across the Tube Arrays

Differential pressure transducer supplied by Flow Kinetics was used to measure directly the air pressure drop across the array, ΔP_a. For both circular and elliptical arrays two pairs of pressure taps located at the same level upstream and downstream of the tubes array were connected to the pressure transducer to read the air side pressure loss. The locations of the pressure taps are displayed in figure 3.2.

3.3.3 Measurements of the Water Flow Rate

The water flow rate was measured using an inline flow meter located at the inlet of the tube array. The flow meter was calibrated over the flow range considered in the study before taking the actual measurements.

CHAPTER 4

DATA REDUCTION

The determination of the thermal and hydraulic representations for the performance analysis is shown in this chapter. The data reduction procedure is described in details based on fundamental knowledge of fluid flow and heat transfer.

4.1 Dimensionless Heat Transfer and Fluid Mechanics Numbers

In fluid mechanics and heat transfer analysis, a set of dimensionless numbers are extensively used. These numbers allow relationships between different parameters to be established and hence results to be generalized for a broad range of applications. Heat transfer rate as relevant to flow conditions is generally presented in the non-dimensional form of Nusselt number, Nu, or Stanton number, St, as a function of Reynolds number, Re, and Prandtl number, Pr. As similar to the heat transfer, the pressure drop as a common practice is obtained in dimensionless form associated with different flow conditions. The dimensionless numbers considered in this study are defined in details below.

Reynolds Number

The Reynolds number, Re, is named after the British scientist, Osborn Reynolds, who in 1880s was the first to reveal that combination of variables can be used as a standard to characterize a fluid flow into different regimes, laminar and turbulent. Reynolds number governs the flow in force convection. It is defined as the ratio of inertia force to viscous force for a particular flow condition. It is expressed in the following general form:

$$\mathrm{Re} = \frac{\text{Inertia Force}}{\text{Viscous Force}} = \frac{\rho\, VZ}{\mu} \tag{4.1}$$

where ρ is the fluid density, V is the reference velocity, Z is the characteristic length, μ is the dynamic viscosity. At low values of Reynolds number, viscous force is dominated over inertia force leading to a smooth motion characterizes the laminar flow .Whereas, inertia force dominates the flow at high Reynolds number, resulting in a turbulent flow characterized by disordered motion (Munson et al. 2002).

Prandtl Number

The Prandtl number, Pr, is named in honour of the German scientist, Ludwig Prandtl, who in 1904 presented the concept of the boundary layer. It is defined as the ratio of momentum diffusivity to thermal diffusivity of a fluid. It is normally presented in the following form:

$$\mathrm{Pr} = \frac{\text{Momentum diffusivity}}{\text{Thermal diffusivity}} = \frac{\nu}{\alpha} = \frac{\mu/\rho}{k/\rho\, c_p} = \frac{\mu\, c_p}{k} \tag{4.2}$$

where ν is the kinematic viscosity, α is the thermal diffusivity, c_p is the specific heat, and k is the thermal conductivity. The above definition shows that Prandtl number depends only on the fluid and its state. Thus, Prandtl number is solely a fluid property.

Prandtl number is used to measure the development of the velocity boundary relative to the thermal boundary layer in heat convection analysis. As described by Çengel (2007), the shape of the temperature profile in the thermal boundary layer has a significant effect on the rate of heat convection between a surface (e.g. a cylinder wall) and a flowing fluid. Since the flow velocity strongly influences the temperature profile, the thickness of the velocity boundary layer relative to thermal boundary layer has a vital role on the convection heat transfer. In fluids with Pr << 1, heat diffuses relative to momentum, and hence the thermal boundary layer is much thicker relative to the velocity boundary layer. On the other hand, in fluids with Pr >> 1 heat dissipates through the fluid very slowly, therefore, the velocity boundary layer is much thicker than the thermal boundary layer. In the case of Pr ≈ 1, heat diffuses through the fluid at the same rate as the momentum (Çengel 2007).

Grashof Number

The Grashof number, Gr, is named after the German engineer, Franz Grashof. It represents the ratio of the buoyancy force to the viscous force acting on the fluid. It is generally defined in the following form:

$$\mathrm{Gr} = \frac{\text{Buoyancy Force}}{\text{Viscous Force}} = \frac{g\beta\left(\left|T_s - T_\infty\right|\right)Z^3}{\nu^2} \tag{4.3}$$

where β is the volumetric thermal expansion [$\beta = \dfrac{1}{T+273}$, where $T = T_f$ for air side, and $T = T_{w_b}$ for water side], g is the gravitational acceleration, coefficient, T_∞ is the free stream temperature, and Z is the characteristic length. Grashof number in natural convection plays the same role as Reynolds number in forced convection. It governs the flow regime in natural convection. In another word, Grashof number is used as a criterion to determine whether the flow is laminar or turbulent (Çengel 2007).

According to Incorporeal and DeWitt (2002), and Çengel (2007), in heat convection applications, natural convection is always present alongside with force convection. This is a result of the gravity effect on a flowing fluid accompanied with temperature gradient. In convection heat transfer the fluid velocity has a strong influence on the heat transfer coefficient. Fluid velocity in forced convection is higher compared to natural convection. Therefore, forced convection heat transfer coefficient is much higher than that of the natural convection. Consequently, in forced convection analysis, the effect of natural convection is usually neglected, mainly, at high velocities. In view of that, the non- dimensional parameter $\mathrm{Gr}/\mathrm{Re}^2$ is used to assess the effect of natural convection as relative to forced convection. When $\mathrm{Gr}/\mathrm{Re}^2 < 0.1$, the natural convection effect is insignificant which means heat transfer is dominated by forced convection. Whereas the effect of forced convection is negligible if $\mathrm{Gr}/\mathrm{Re}^2 > 10$.

Nusselt Number

The Nusselt number, *Nu*, named after the German scientist Wilhelm Nusselt, is a dimensionless representation of the heat transfer coefficient, *h*. In heat transfer between a solid surface and a flowing fluid, Nusselt number is interpreted as the ratio of convective to conductive heat transfer within the fluid. It is generally defined as

$$\mathrm{Nu} = \frac{Q_{conv}}{Q_{cond}} = \frac{h\,Z}{k} \tag{4.4}$$

where Q_{conv} is the rate of convection heat transfer, Q_{cond} is the rate of conduction heat transfer, h is the heat transfer coefficient, and Z is the characteristic length .

Heat transfers by convection through a fluid layer when the fluid is in motion. On the contrary, heat transfers by conduction when the fluid is at rest. Thus, to enhance heat transfer within the fluid, increasing the rate of heat convection relative to conduction is required. A Nusselt number of about unity means the convection and conduction are of similar magnitude. A larger Nusselt number indicates that the convection is more active as relative to the conduction (Incropera and DeWitt 2002).

Stanton Number

The Stanton number denoted as St is also a dimensionless representation of the heat transfer coefficient. It is named after Thomas Edward Stanton, a British scientist. Stanton number represents the ratio of heat convection to the enthalpy rate change of the fluid approaching a temperature of solid surface. It is expressed as

$$\mathrm{St} = \frac{h\,A\left(T_s - T_\infty\right)}{G\,A_o\,c_p\left(T_o - T_i\right)} = \frac{h}{G\,c_p} = \frac{h}{\rho\,\mathrm{V} c_p} \tag{4.5}$$

where A is the duct surface area, A_o is the flow cross sectional area, G is the fluid mass velocity, T_i is the fluid inlet temperature, and T_o is the fluid outlet temperature.

The Stanton number is generally preferred to the Nusselt number as a dimensionless heat transfer coefficient when the axial heat conduction of the fluid is negligible. This is because the Stanton number direct relation to the number of transfer units, NTU. In addition, the Stanton number variation with Reynolds number is similar to the behaviour of the fanning friction factor or the pressure drop coefficient with Reynolds number; they vary inversely with Reynolds number. Besides, Stanton number, unlike Nusselt number, as defined in Eq. (4.5) is independent of the characteristic length (Shah and Sekulić 2003).

The Stanton number is related to the Nusselt number, Prandtl number, and Reynolds number through the following definition:

$$\mathrm{St} = \frac{\mathrm{Nu}}{\mathrm{Re}\,.\,\mathrm{Pr}} \tag{4.6}$$

Eq. (4.6) is always valid for any flow condition, geometry, and (Shah and Sekulić 2003).

4.2 Heat Transfer Correlations

Fluid flow across tubes of various shapes (e.g. circular and elliptical) is commonly encountered in industrial applications. Tubular cross flow heat exchangers, as an example, involve both external flow over the exterior surface of the tubes and internal flow inside the tubes. Therefore, in heat exchangers performance analysis, flow in both sides should be considered. Flow pattern across a tube or tubes is very complicated and significantly controls the heat transfer from or to such bodies. Accordingly, experimental and numerical techniques must be used to study the fluid flow and heat transfer around such objects.

Several experimental investigations in this area have been reported in the available literatures. Heat transfer data obtained from these studies, as common practice, are presented in dimensionless correlations of Nu or St as a function of Re and other parameters. Heat transfer for a single tube, a tube in a single row or bank, or for a single row of tubes is mainly dependent on the velocity of the incoming fluid, properties of the thermal carrier, tube arrangement, intensity and direction of heat transfer. As suggested by Žukauskas (1972) and Žukauskas and Ulinskas (1988), and using the definition of St as of Eq. (4.6), this correlation in a dimensionless form is defined as of Eq. (4.7) below.

$$\mathrm{Nu\ or\ St} = f\left(\mathrm{Re}, \mathrm{Pr}, \frac{\mu}{\mu_s}, \frac{k}{k_s}, \frac{c_p}{c_{p_s}}, \frac{\rho}{\rho_s}, \frac{S_T}{Z}\right) \tag{4.7}$$

where Z represents the characteristic length, and μ, k, c_p, and ρ, and represents the dynamic viscosity, the thermal conductivity, the specific heat, the density of the main flow, respectively. The subscript s indicates that the fluid property is evaluated at the surface temperature.

For the flow of air over tubes, external flow, the last term in the parentheses in Eq. (4.7), S_T/Z, is a geometric characteristic. It accounts for the variation of the tubes arrangement at the airside. Since there were no changes applied in the tubes arrangement in the present study, this term was ignored. As a result, Eq. (4.7) can be simplified in term of Nu as a function of the main parameters, Re and Pr, as

$$\mathrm{Nu} = \mathrm{a}\ \mathrm{Re}^{\mathrm{b}}\ \mathrm{Pr}^{\mathrm{n}}\ \left(\mathrm{Pr}/\ \mathrm{Pr}_s\right)^{\mathrm{p}} \tag{4.8}$$

, and when St is included Eq. (4.8) can be written as

$$\mathrm{St} = \mathrm{c}\ \mathrm{Re}^{\mathrm{b-1}}\ \mathrm{Pr}^{n-1}\ \left(\mathrm{Pr}/\ \mathrm{Pr}_s\right)^{\mathrm{p}} \tag{4.9}$$

where the values of the coefficient c, and the exponents m, n and p are to be determined based on experimental data. The value of the exponent n is usually set equal to 1/3 (Žukauskas 1972). The parameter $\left(\mathrm{Pr}/\ \mathrm{Pr}_s\right)^p$ in the above equation is introduced to account for the effect of the temperature head and the direction of the heat flow. For gases in general and air in particular this parameter is equal to unity. This is due to the fact that Pr is nearly constant around the wall and outside the boundary layer for moderate temperature range (Žukauskas and Ulinskas 1988). Therefore, Eq. (4.8) and Eq. (4.9) can be re-written as

$$\mathrm{Nu} = \mathrm{a}\ \mathrm{Re}^{\mathrm{b}}\ \mathrm{Pr}^{1/3} \tag{4.10}$$

$$\mathrm{St} = \mathrm{c}\ \mathrm{Re}^{\mathrm{b-1}}\ \mathrm{Pr}^{-2/3} \tag{4.11}$$

In the case that Pr considered constant within a set of experimental conditions, Eq. (4.10) and Eq. (4.11) can be further simplified as follows

$$Nu = a_1 \, Re^{b} \tag{4.12}$$

$$St = c_1 \, Re^{b-1} \tag{4.13}$$

As mentioned at the beginning of this thesis, the primary interest of the current study was to investigate the air flow heat transfer features. However, as another interest, the heat transfer characteristics for the water flow inside the tubes were also studied. The results were correlated in term of Nu variations with Re and Pr. Within the conditions considered in the current study, Eq. (4.12) was used to present the water flow heat transfer results.

4.3 Dimensionless Representation of Air Side Pressure Drop

Pressure drop across a tube or an array of tubes is an essential quantity that affects the overall design of any heat exchanger. It is an indication of the resistance that a fluid passes over tube or an array of tubes encounters. In another word, it is a measure of the power required to drive the flow over such objects (the less pressure drop encountered, the less power required is).

Parallel to the heat transfer correlations, the pressure drop features are usually shown in dimensionless pressure drop coefficient correlated with different Reynolds number. The pressure drop coefficient, P_{dc}, as defined below in Eq. (4.13) represents the ratio of the irreversible pressure drop of the moving air over the tube array to its dynamic pressure ((Merker and Hanke 1986; Gaddis and Gnielinski 1997).

$$P_{dc} = \frac{2\,\Delta P_a}{\rho_a\, V_{max}^2} \tag{4.13}$$

where ΔP_a signifies the pressure drop across the array measured by a pressure transducer connected between a pair of pressure taps as displayed in figure 3.2, ρ_a is the air density evaluated at the bulk air temperature, and V_{max} is maximum velocity at the minimum cross section obtained from Eq. (4.16) and Eq. (4.17).

4.4 Data Reduction

The following assumptions were taking into consideration in the current study:

- Steady state flow is assumed for the air and water flow. Sufficient time was allowed for both sides to reach the steady state condition about 40 to 50 minutes.
- Forced convection is the only mode of heat transfer exists.
    a. The effect of natural convection heat transfer was omitted from the analysis. During the experiment, the ratio Gr / Re^2 was always << 0.1 which validate the neglecting of natural convection.
    b. The heat losses form or to the room were also omitted. The test section walls were made of thick Plexiglas with low thermal conductivity, and there was no temperature difference between the outside air and the test section walls.
    c. Within the considered operating conditions, there was no radiation heat transfer inside the test section.
- The velocity and temperature are uniform over the inlet cross section for air and water flow.

4.4.1 Fluid Flow Data Reduction

Air Flow Reynolds Number

The air flow Reynolds number was calculated from Eq. (4.1) where for flow over the circular tube array, the tube outer diameter, D_o, was used as the characteristic length. While, for the tube outer major axis, $2a_o$, was used in the case of elliptical tube array. Eq. (4.14) and Eq. (4.15) below in sequence represents Re_a for the flow over the circular and elliptical arrays.

$$Re_a = \frac{\rho_a \, V_{a_{max}} \, 2a_o}{\mu_a} \tag{4.14}$$

$$Re_a = \frac{\rho_a \, V_{a_{max}} \, D_o}{\mu_a} \tag{4.15}$$

where $V_{a_{max}}$ is the maximum velocity at the minimum cross section (the area between any two adjacent tubes) and was calculated as suggested by Buyruk (1999) and Castiglia et al. (2001) as in Eq. (4.16) for the circular tube array and Eq. (4.16) for the elliptical one.

$$V_{a_{max}} = \frac{S + D_o}{S} V_a \tag{4.16}$$

$$V_{a_{max}} = \frac{S + 2b_o}{S} V_a \tag{4.17}$$

Where V_a is air inlet velocity calculated from Eq. (3.1) and S is the gab between the outer surfaces of any two adjacent tubes.

Water Flow Reynolds Number

The water flow Reynolds number, Re_w, was calculated from Eq. (4.1) where the inlet water velocity, V_w, estimated from Eq. (4.19) was used as a reference velocity and the inner hydraulic diameter, D_{h_i}, was used as the characteristic length. Eq. (4.18) below was used to estimate the Re_w for the circular and elliptical arrays.

$$Re_w = \frac{\rho_w V_w D_{h_i}}{\mu_w} \tag{4.18}$$

$$V_w = \frac{FR_w}{A_i} \tag{4.19}$$

4.4.2 Heat Transfer Data Reduction

Heat Transfer Rate

The overall air and water heat transfer rate, Q, was used to determine the average heat transfer coefficient for the air, h_a, and water, h_w. According to Shah and Sekulić (2003) to account for imbalances in the water and air heat transfer rates, Q_w and Q_a, respectively, Q is generally reduced based on the arithmetic average of both streams heat transfer rates. An energy balance was made to reduce the water and air flow heat transfer rates. Accordingly, Q_w, Q_a and Q were estimated as shown in Eq. (4.20), Eq. (4.21), and Eq. (4.22), respectively.

$$Q_w = m_w c_{p_w} (T_{w_i} - T_{w_e}) \tag{4.20}$$

$$Q_a = m_a c_{p_a} (T_{a_e} - T_{a_i}) \tag{4.21}$$

$$Q = \frac{Q_w + Q_a}{2} \tag{4.22}$$

where c_{p_w} , c_{p_a} in sequence are the water and air specific heats (evaluated at the fluid bulk temperature), and m_w , m_a as defined in Eq. (4.23) and Eq. (4.24) are the water and air flow rates, respectively.

$$m_w = \rho_w \text{ FR} \tag{4.23}$$

$$m_a = \rho_i \text{ V}_a \text{ A}_i \tag{4.24}$$

Air Flow Average Heat Transfer Coefficient

The average heat transfer coefficient for the air flow, h_a, was estimated from the Newton's Law of cooling as follows

$$h_a = \frac{Q}{A_{s_o}(T_s - T_{a_i})} \tag{4.25}$$

Based on h_a , Nu_a was reduced from Eq. (4.4). As in the definition of Re_a, D_o and $2a_o$ were used as the characteristic lengths to define Nu_a as in Eq. (4.24) and Eq. (4.24), respectively.

$$Nu_a = \frac{h_a D_o}{k_a} \tag{4.26}$$

$$Nu_a = \frac{h_a 2a_o}{k_a} \tag{4.27}$$

St_a was also estimated from h_a from Eq. (4.5) for the flow over the circular and the elliptical tube arrays as follows

$$St_a = \frac{h_a}{\rho_a V_{a_{max}} c_{p_a}} \tag{4.28}$$

Water Flow Average Heat Transfer Coefficient

Similar to the air flow, the average heat transfer coefficient for the water flow, h_w, was estimated from the Newton's Law of cooling as follows

$$h_w = \frac{Q}{A_{s_i}(T_{w_b} - T_s)} \tag{4.29}$$

Based on the above equation, Nu_w was estimated for the flow inside the tubes for both the circular and the elliptical arrays from Eq. (4.4). D_{h_i} was used to define Nu_w as in Eq. (4.28) below

$$Nu_w = \frac{h_w D_{h_i}}{k_w} \tag{4.30}$$

CHAPTER 5
RESULTS AND DISCUSSIONS

5.1 Effect of Reynolds Number on Heat Transfer for the Air Stream

In order to establish a relationship between the average air flow heat transfer of circular and elliptical tube arrays and the air velocity, the effect of the Reynolds number on the Nusselt and Stanton numbers was observed. The air flow Reynolds and Nusselt and Stanton numbers were reduced as described in sections 4.4.1 and 4.4.2, respectively. A number of test runs were performed on both tube arrays. Results based on the collected experimental data are shown in this section.

Figures 5.1 and 5.2 show the heat transfer results as a function of Reynolds number for the circular tube array. Air was forced to flow over the array at six different Reynolds number ranging from 17100 to 48500, and exchange heat with water at different flow rate varying from 0.01 to 0.11 kg/s. As a result, a set of equations in term of Nu_a and St_a variations with Re_a were generated based on Eq. (4.12) and Eq. (4.13). The results are tabulated in table 5.1.

Table 5.1 Nu_a and St_a as a function of Re_a at different water flow rate for the case of the circular tube array.

m_w [kg/s]	Circular tube array	R^2	Circular tube array	R^2
0.01	$Nu_a = 0.160\ Re_a^{0.599}$	0.97	$St_a = 0.317\ Re_a^{-0.439}$	0.94
0.02	$Nu_a = 0.160\ Re_a^{0.596}$	0.94	$St_a = 0.185\ Re_a^{-0.385}$	0.94
0.04	$Nu_a = 0.168\ Re_a^{0.592}$	0.96	$St_a = 0.167\ Re_a^{-0.377}$	0.92
0.07	$Nu_a = 0.209\ Re_a^{0.572}$	0.96	$St_a = 0.292\ Re_a^{-0.430}$	0.97
0.11	$Nu_a = 0.117\ Re_a^{0.628}$	0.97	$St_a = 0.239\ Re_a^{-0.410}$	0.93

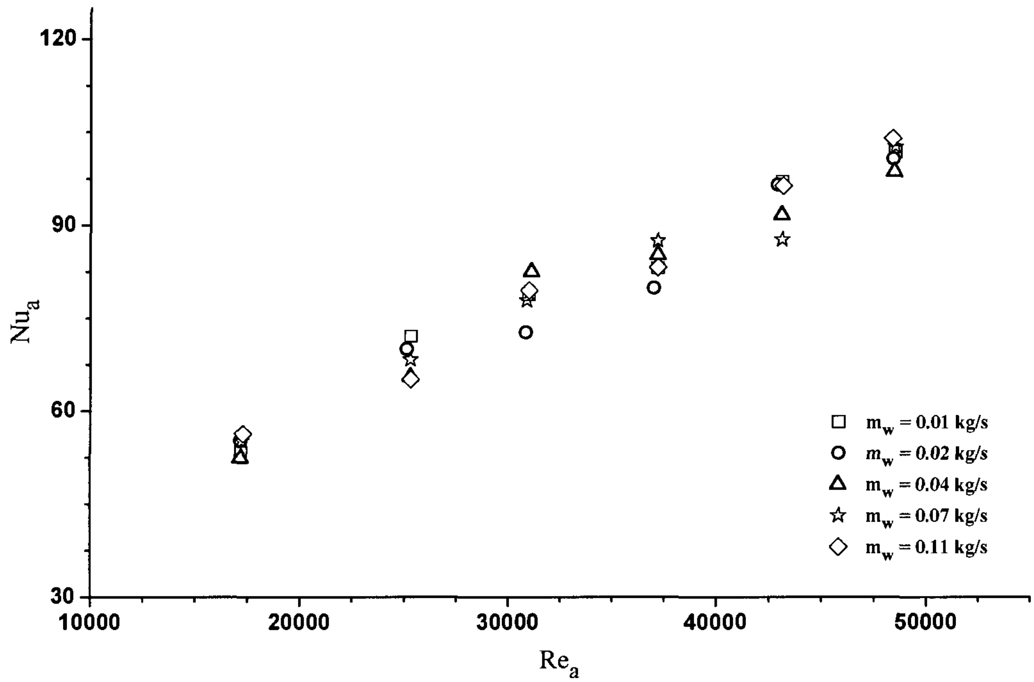

Figure 5.1 Nu_a as a function of Re_a for different water flow rate for the case of the circular tube array

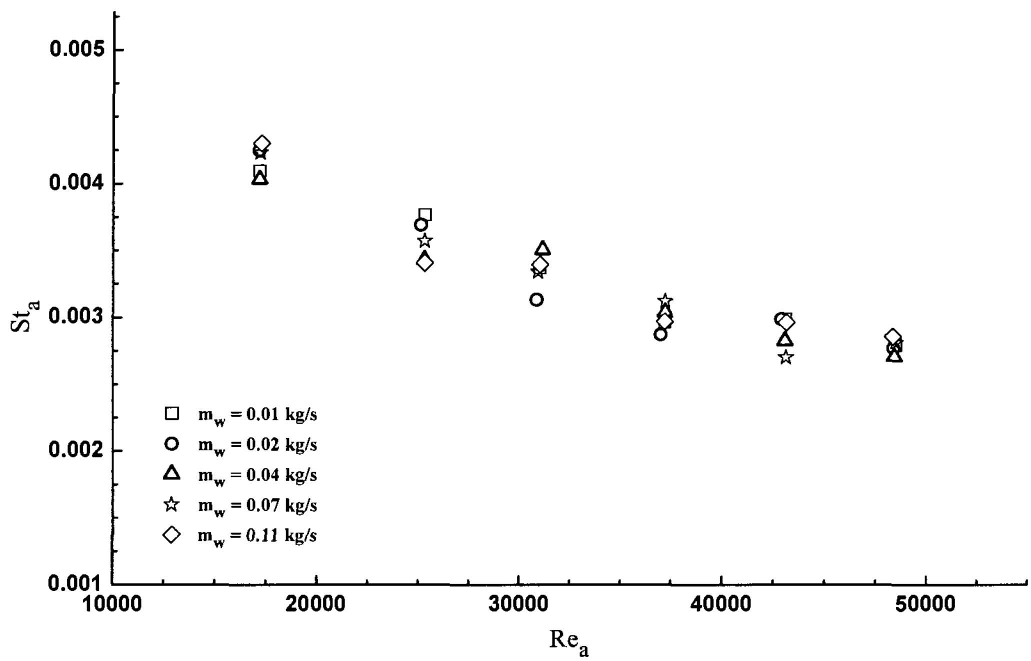

Figure 5.2 St_a as a function of Re_a for different water flow rate for the case of the circular tube array

The variations of the air flow Nusselt and Stanton numbers with Reynolds number for the elliptical tube array are shown below in figures 5.3 and 5.4. The air was forced to flow within similar conditions to that applied to the circular tube array. The Reynolds number was varied in six steps from 17000 to 49400, while the water was flowing at the same rate as in the circular tube array case, 0.01 to 0.11 kg/s. In accordance with Eq. (4.12) and Eq. (4.13), a relationship in the form of Nu_a and St_a dependency on Re_a was obtained. The results are presented in 5.2 below.

Table 5.2 Nu_a and St_a as a function of Re_a at different water flow rate for the case of the elliptical tube array.

m_w [kg/s]	**Elliptical tube array**	**R^2**	**Elliptical tube array**	**R^2**
0.01	$Nu_a = 0.208\ Re_a^{0.627}$	0.95	$St_a = 0.289\ Re_a^{-0.373}$	0.92
0.02	$Nu_a = 0.346\ Re_a^{0.576}$	0.95	$St_a = 0.541\ Re_a^{-0.422}$	0.97
0.04	$Nu_a = 0.260\ Re_a^{0.601}$	0.96	$St_a = 0.359\ Re_a^{-0.400}$	0.93
0.07	$Nu_a = 0.466\ Re_a^{0.542}$	0.97	$St_a = 0.377\ Re_a^{-0.402}$	0.92
0.11	$Nu_a = 0.241\ Re_a^{0.609}$	0.97	$St_a = 0.202\ Re_a^{-0.343}$	0.94

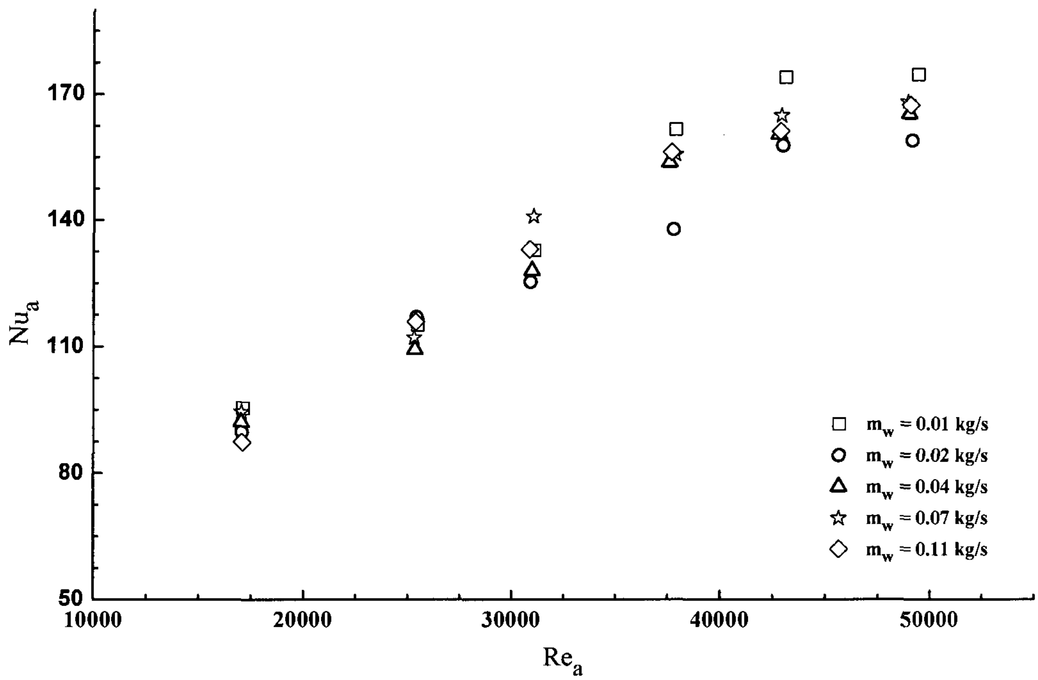

Figure 5.3 Nu_a as a function of Re_a for different water flow rate for the case of the elliptical tube array

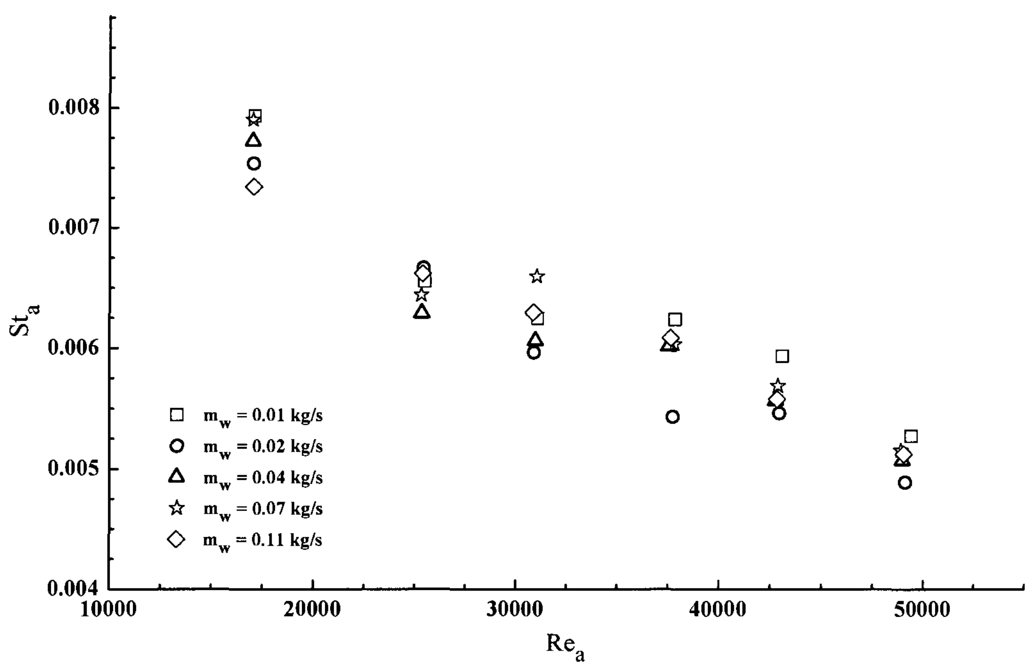

Figure 5.4 St_a as a function of Re_a for different water flow rate for the case of the elliptical tube array

Figures 5.1 and 5.3 above portray the air flow Nu_a as a function of Re_a for the circular and elliptical tube arrays, respectively. The curves were generated for different water flow conditions. The results show that for given water flow rate, increasing Re_a results in an increase in Nu_a in a power law form for both circular and elliptical arrays for the entire range of Re_a considered. Water flow rate was varied in five steps with different air flow to observe the effect of the water side flow rate in the average heat transfer rate at the air side. From the obtained curves, it is obvious that the water flow rate has no effects on the heat transfer results for the air flow. The Nu_a values were nearly unchanged for the entire flow range investigated. The average heat transfer for the air flow it was rather influenced by the air flow rate. This is attributed to the high thermal resistance at the air side which is always greater than that of the water side.

Plotted in figure 5.2 are the heat transfer results in term of St_a variations with Re_a for different water flow rate for the circular tube array. For elliptical arrays of tubes the results obtained are presented in figure 5.4. It is observed that for a fixed water flow rate, the St_a decreases in an inverse power law form as Re_a increases. The St_a decreases in the same manner with Re_a for the entire water flow rate covered. All the figures above show that the change in St_a is only dominated by the change in Re_a. This is again because of the high heat transfer resistance from the external flow of air.

From the results shown in table 5.1 and 5.2 and displayed in the figures above, overall heat transfer correlations were obtained in term of Nusselt and Stanton with their dependency on Reynolds number. For the current study, Prandtl number for the air flow, Pr_a, was nearly constant (≈ 0.73). Accordingly, two separate correlations were established for each of the tube array based on Eq. (4.12) and Eq. (4.13) as follows

The correlation in term of Nu_a variation with Re_a for the circular tube array is:

$$Nu_a = 0.162\ Re_a^{0.596} \qquad , R^2 = 0.94 \tag{5.1}$$

and for the elliptical tube array is:

$$Nu_a = 0.288\ Re_a^{0.592} \qquad , R^2 = 0.94 \tag{5.2}$$

The correlation in term of St_a variation with Re_a for the circular tube array is:

$$St_a = 0.241\ Re_a^{-0.412} \qquad , R^2 = 0.92 \tag{5.3}$$

and for the elliptical tube array is:

$$St_a = 0.334\ Re_a^{-0.392} \qquad , R^2 = 0.92 \tag{5.4}$$

The obtained correlations are applicable for Reynolds number in the range of 17000 to 49000.

Figure 5.5 portrays Nusselt number variation with respect to Reynolds number for the circular and elliptical tube arrays. As expected, the results show that at low Reynolds number, the thermal resistance of the air is high. Thus, low Nusselt number was obtained. The experimental results illustrate that the Nusselt number constantly increases as Reynolds number increases for both arrays. The trend is the heat transfer of the circular tube array is always lower than that of the elliptical tube array.

Figure 5.6 presents the Stanton number as a function of Reynolds number for both arrays. The results show that for a fixed flow condition, the elliptical tube array provided higher heat transfer in term of Stanton number than that obtained by the circular tube one. The Stanton number always decreases as Reynolds number. Based on the definition of Stanton number in Eq. (4.5), this is attributed to the nature of the thermal and velocity boundary layer development. In another word, at high Reynolds numbers the heat convective from the tubes to the surrounding air increases slower than the air velocity.

As depicted in figure 5.6 and 5.6, it is clear that the elliptical tube array predicted higher heat transfer than that of the circular tube array. Based on the above correlations, the utilization of elliptical tubes provided roughly 70 % of relative enhancement in the heat transfer as compared to the circular tubes. This heat transfer gain is a result of the slender shape of the elliptical tube. The elliptical tubes used in this study were made by reforming circular tubes with same dimensions as the ones used in the circular tube array. They were manufactured to have axis ratio of 0.3 compared to 1 for the circular tubes. This allows 18 elliptical tubes to be utilized in the same space as compared to 10 circular tubes. Therefore, the surface area per unit volume increases resulting in better heat transfer rate.

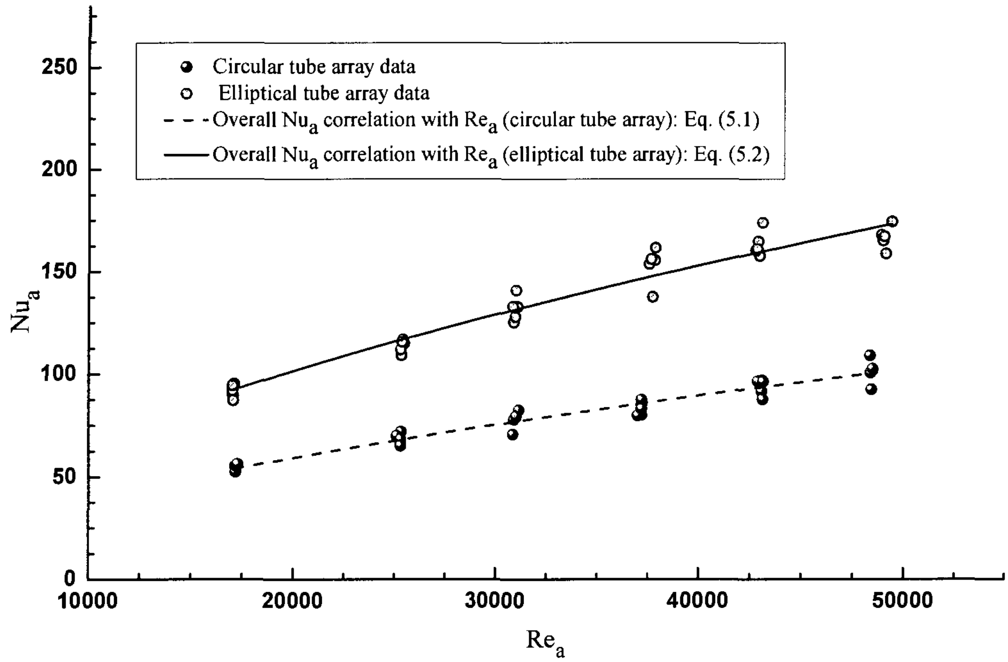

Figure 5.5 Overall Nu_a vs Re_a (circular vs elliptical)

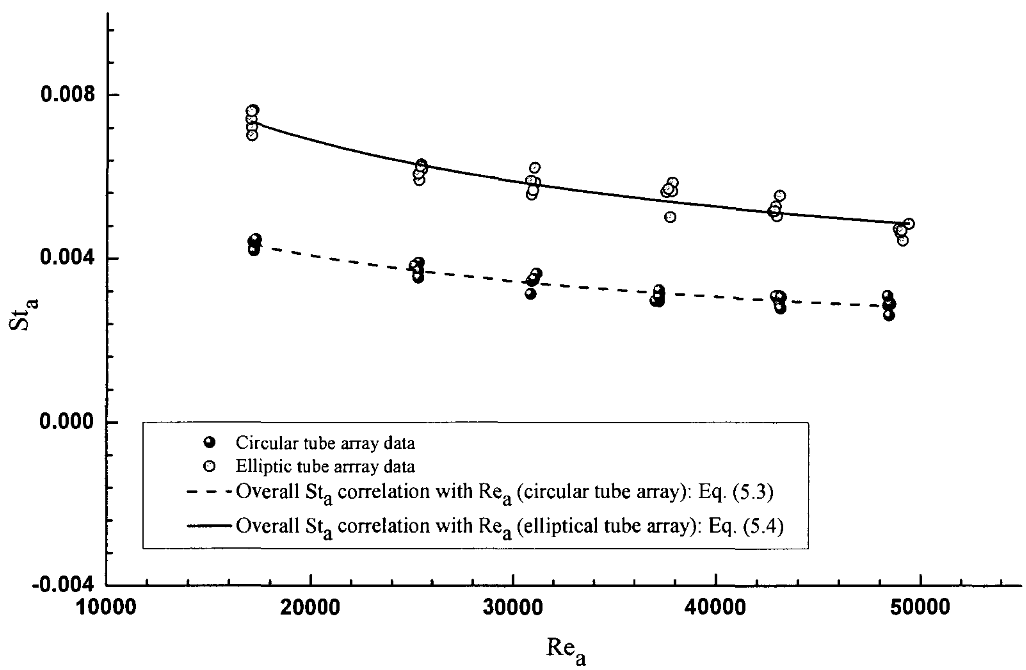

Figure 5.6 Overall St_a vs Re_a (circular vs elliptical)

5.2 Comparison of the Present Air Flow Heat Transfer Results with Others from the Literature

The Nu_a and St_a correlations with Re_a obtained from the present study are compared below with other results from previous studies as shown in figures 5.7 through 5.10.

Figures 5.7 and 5.8 show comparisons of the current proposed heat transfer correlations for the circular tube array, Eq. (5.1) and Eq. (5.3), with others found in the literatures. One general correlation based on the experimental work of Žukauskas (1972) as referenced by Çengel, Y. A. (2007) in the following form:

$$Nu_a = 0.27\, Re_a^{0.63} Pr_a^{0.36} (Pr_a / Pr_s)^{0.25} \qquad (1000 \leq Re_a \leq 200000) \qquad (5.5)$$

where Pr_a is evaluated at the air flow bulk temperature, and Pr_s is evaluated at the surface temperature. This correlation can be applied for fluid with Prandtl number ranging from 0.7 to 500 and flow over circular tube banks having more than 16 rows of tubes. To apply this equation on a single inline circular tube array, a correction factor equal to 0.7 is introduced. By introducing this factor and other parameters form the present study, the above equation can be written as follows

$$Nu_a = 0.169\, Re_a^{0.63} \qquad (17000 \leq Re_a \leq 49000) \qquad (5.6)$$

from the definition of Stanton number, Eq. (4.6), Eq. (5.6) can be rewritten as

$$St_a = 0.232\, Re_a^{-0.37} \qquad (17000 \leq Re_a \leq 49000) \qquad (5.7)$$

Another empirical correlation was established by Grimison (1937) for circular tube banks with more than 10 rows. It is written as

$$Nu_a = 0.32\, Re_a^{0.61} Pr_a^{0.31} \qquad (5.8)$$

including a row correction factor equal to 0.64 and applying the current experimental condition, the above equation can be used for an inline array of tube in the following form:

$$Nu_a = 0.186\ Re_a^{0.61} \qquad (17000 \le Re_a \le 49000) \qquad (5.9)$$

introducing the Stanton number as defined in Eq. (4.6) into the Eq. (5.9), gives a correlation in term St_a of as

$$St_a = 0.255\ Re_a^{-0.39} \qquad (17000 \le Re_a \le 49000) \qquad (5.10)$$

As seen in figures 5.7, and 5.8, the correlations from the present study have satisfactory agreement with that proposed by Grimison and Žukauskas. However, for a fixed Re_a, the current proposed correlations estimated relatively lower heat transfer than obtained by Žukauskas' and Grimison's by 45 % and 32 %, respectively. This discrepancy could be attributed to the difference in the arrangement of the tubes and the experimental conditions applied.

The Nu_a and St_a correlations obtained for the elliptical tube array, Eq. (5.2) and Eq. (5.4), are plotted in figure 5.9 and 5.10 with the experimental results of Žukauskas (1972) and Ibrahim and Gommah (2009). Žukauskas (1972) found that the heat transfer from a single elliptical tube in cross flow of air can be correlated by the generalized equation as

$$Nu_a = 0.27\ Re_a^{0.60} Pr_a^{0.37} (Pr_a/Pr_s)^{0.20} \qquad (1000 \le Re_a \le 200000) \qquad (5.11)$$

where Pr_a is evaluated at the air flow bulk temperature, and Pr_s is evaluated at the surface temperature. In this correlation Reynolds number is defined based on the major axis length of the tube. Eq. (5.11) is applicable for uniform heat flux and isothermal surface boundary conditions. By introducing the conditions from present study, Eq. (5.11) will take the following form:

$$Nu_a = 0.240\ Re_a^{0.60} \qquad (17000 \leq Re_a \leq 49000) \qquad (5.12)$$

in term of Stanton number, Eq. (5.12) can be rewritten as

$$St_a = 0.329\ Re_a^{-0.4} \qquad (17000 \leq Re_a \leq 49000) \qquad (5.13)$$

Ibrahim and Gomma (2009) proposed a heat transfer correlation for elliptical tube bundle in cross flow of air in the following form:

$$Nu_a = 0.452\ Re_a^{0.537}\ Pr_a^{0.33}\ (b/a)^{-0.079}(\sin(10+\alpha))^{0.2} \qquad (5.14)$$

where a and b are the semi major and minor axis of the elliptical tube, and α is the flow angle of attack. This correlation is valid for a range of Reynolds number from 5300 to 28000. The hydraulic diameter was used to define Reynolds number in Eq. (5.14). By applying the current experimental condition and using the major axis to define Reynolds number, Eq. (5.14) can be reduced to

$$Nu_a = 0.315\ Re_a^{0.537} \qquad (17000 \leq Re_a \leq 49000) \qquad (5.15)$$

based on the Stanton number, Eq (5.15) can be expressed as

$$St_a = 0.432\ Re_a^{-0.463} \qquad (17000 \leq Re_a \leq 49000) \qquad (5.16)$$

As seen in figures 5.9 and 5.10, the current correlations for the elliptical tube array is in reasonable agreement with that of Žukauskas and Ibrahim and Gomma. The current correlation predicted rather higher Nu_a compared to previous studies. The current estimated Nu_a was in average 10 % and 62 % higher than that estimated by the correlation of Žukauskas and Ibrahim and Gomma, respectively. It is worth mentioning that Žukauskas' correlation was proposed for a single elliptical tube with axis ratio of 0.5

while the current correlation is for a single array of elliptical tube having tubes with axis ratio of 0.3. This difference in the axis ratio a long with the number of the tubes and the experimental conditions applied may have contributed to this little variation in the results.

In general, the correlations proposed in the current study for both circular and elliptical arrays agreed well with the results found in the literature. However, some discrepancies were observed between the results in the present study and those of the previous studies. Factors such as the tube layout, the arrangement of the tubes, and the thermal and flow conditions may cause such variations in the results.

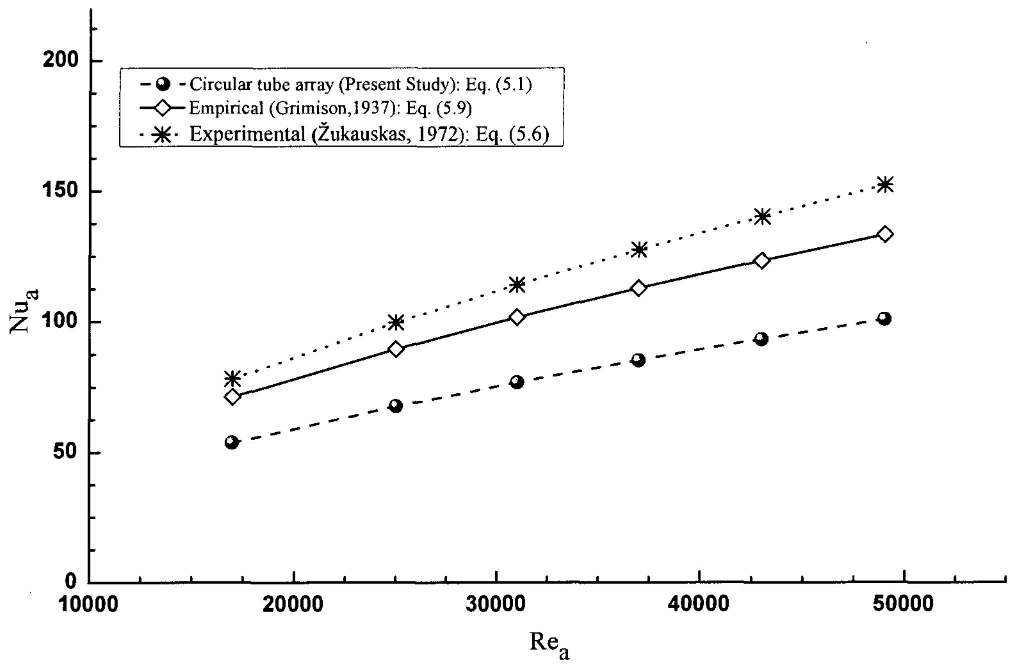

Figure 5.7 Comparison of present overall Nu_a vs Re_a with previous work (circular tube array)

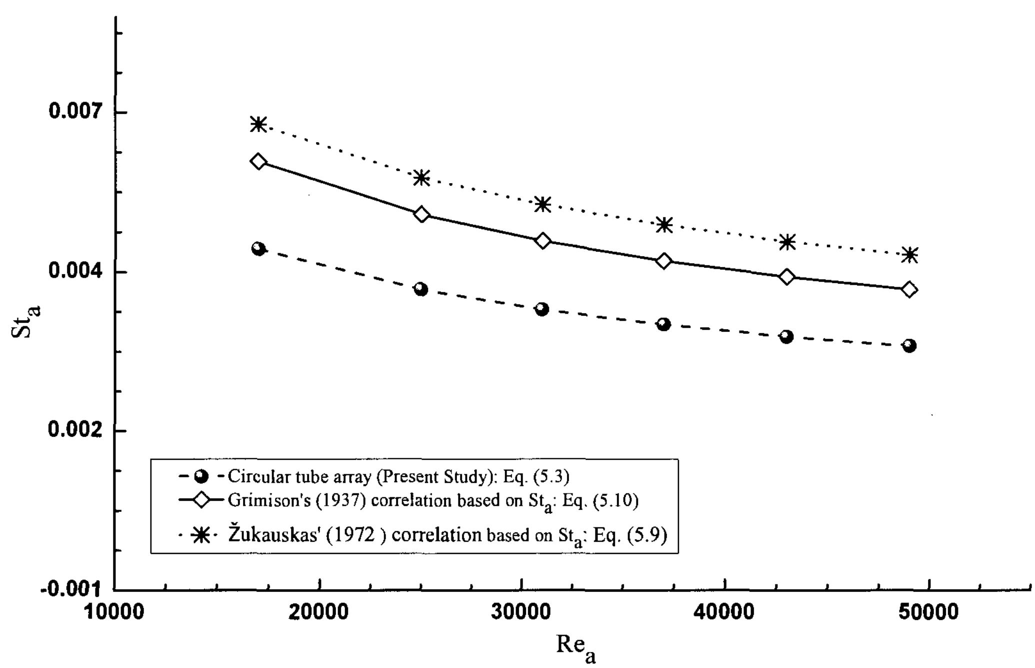

Figure 5.8 Comparison of present overall St_a vs Re_a with previous work (circular tube array)

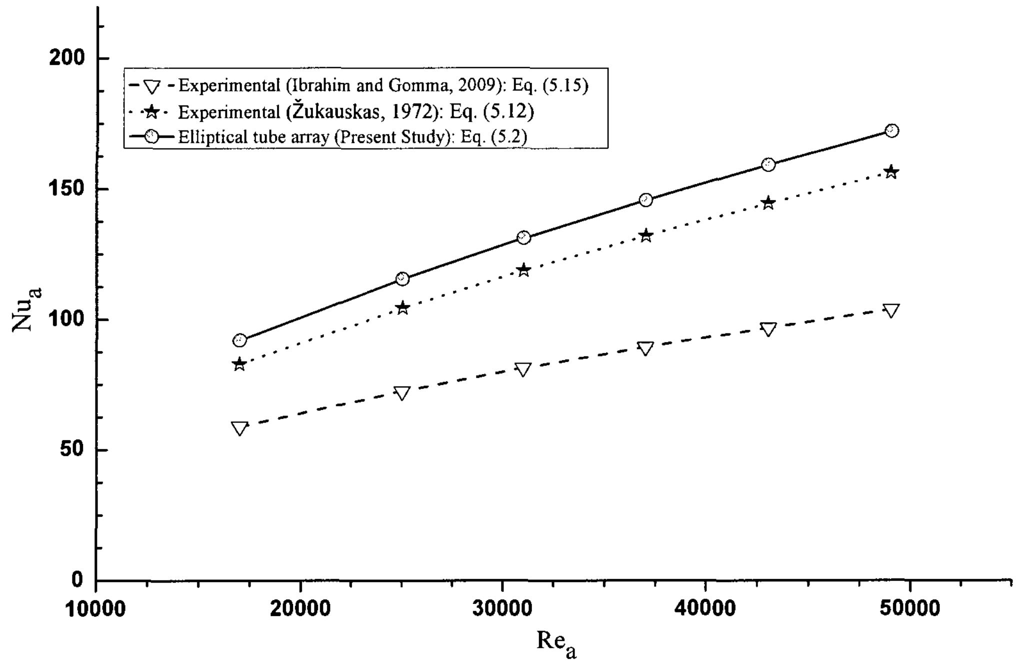

Figure 5.9 Comparison of present overall Nu_a vs Re_a with previous work (elliptical tube array)

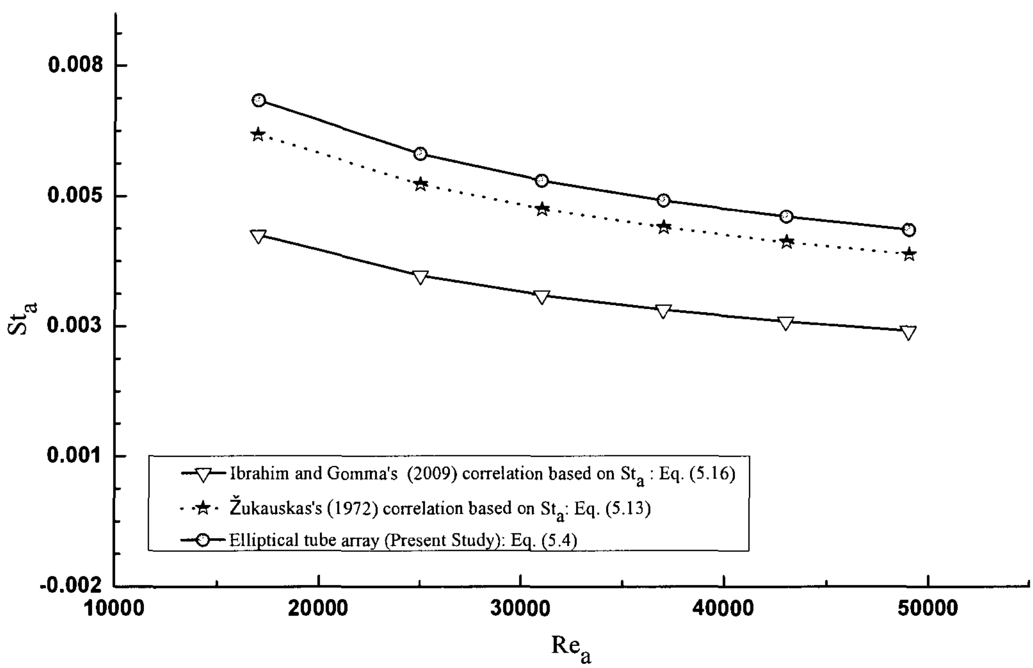

Figure 5.10 Comparison of present overall St_a vs Re_a with previous work (elliptical tube array)

5.3 Air Flow Pressure Drop

The air pressure drop coefficient was estimated based on the detail in section 4.3. In this section, the relation between the pressure drop across the tube arrays and the air flow velocity is established in the dimensionless form of pressure drop coefficient, P_{dc}, as a function of Reynolds number, Re_a. The pressure drop features were investigated for air flow Reynolds number ranging from 17000 to 49000 for the circular and elliptical arrays. To correlate the pressure drop coefficient with Reynolds number, the air flow Reynolds number was varied in six steps with different water flow arte. The experimental data obtained for each tube array was combined in one overall correlation. Eq. (5.17) below represents the correlation for the circular tube array and Eq. (5.18) represent that of the elliptical one.

$$P_{dc} = 2.216\ Re_a^{-0.080} \qquad , R^2 = 0.80 \qquad (5.17)$$

$$P_{dc} = 6.508\ Re_a^{-0.240} \qquad , R^2 = 0.82 \qquad (5.18)$$

Over the experimental conditions considered in the current study, it was observed that the air flow pressure drop was independent of the water flow conditions. Also, the air properties were rather constant. Therefore, the effect of the air temperature was insignificant on the air side pressure drop. It was concluded that only the Reynolds number controls the air flow pressure drop.

Figure 5.11 shows a comparison of the air flow pressure drop coefficient results between the circular and elliptical arrays. As seen, for the range of Reynolds number covered in the present study, the pressure drop coefficient reached a maximum value at the Reynolds number value of 17000. After that, it begun to decrease steadily as Reynolds number increases until reached its minimum value at a Reynolds number of 49000. This is due to the fact that the overall drag consists of two combined parts. One part represents the pressure drag and another one accounts for to the friction drag. At lower Reynolds number, the friction drag is more important than the pressure drag leading to higher pressure drop. In the contrary, at higher Reynolds numbers, the pressure drag is predominant. In this case, the effect of the viscosity is less important and the total drag is rather dominated by the inertia force.

It was also clear that the pressure drop coefficient of the circular tube array is significantly higher than that of the elliptical tube array, by 79 % in average. The low resistance to the flow the elliptical tube array offers is attributed to the tubes layout. The slender shape of the elliptical tubes provides smaller frontal area than that of the circular tubes. This leads to a delay in the separation between the fluid boundary layer and the surface of the tubes. It makes the separation point moves toward the rear stagnation point of the tubes. This makes the size of the weak region behind the tubes smaller and therefore less pressure drop is encountered.

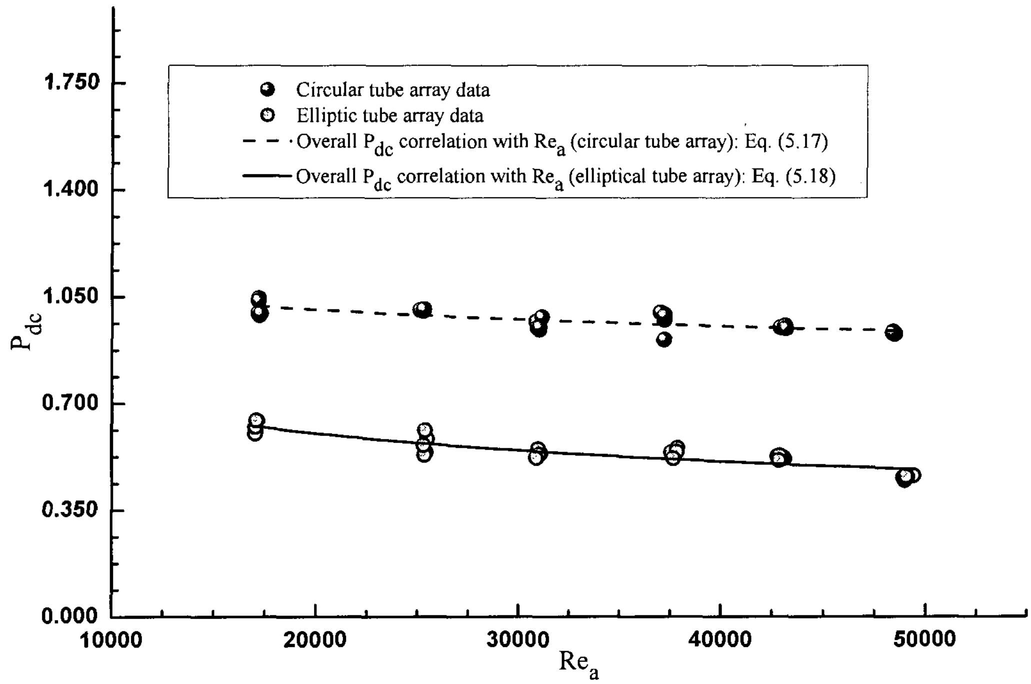

Figure 5.11 Circular and elliptical tube arrays pressure drop comparison

5.4 Comparison of the Present Air Flow Pressure Drop Results with Others from the Literature

The correlations of pressure drop obtained from the present study are compared in figure 5.12 and 5.13 below with the experimental results of Bordalo and Saboya (1999). The study conducted by the above mentioned authors was for elliptical and circular plate fin and tube heat exchangers. The study was for different tube arrangements and different number of tube rows at low flow Reynolds number, 200 to 1800. Their results are as shown below.

For an array consists of two rows of circular tubes, they provided the following correlation:

$$P_{dc} = 1.552\ Re_a^{-0.017} \tag{5.19}$$

And for the a single elliptical tube they suggested a correlation as

$$P_{dc} = 9.769\ Re_a^{-0.303} \tag{5.20}$$

As seen in figures 5.12, the current correlation for the circular tube array is in good agreement with that of Bordalo and Saboya (1999). Within the Reynolds number range considered in the current study, Bordalo and Saboya's correlation predicted relatively higher P_{dc} , in average by 35 %, compared to that of the current correlation. Since the suggested correlation of Bordalo and Saboy was established for an array of two rows of circular finned tube, this variation in the results is reasonable.

From the results shown in figure 5.13, for the Reynolds number range investigated in the current study Bordalo and Saboya's correlation predicted lower P_{dc} , roughly 28 %, as relative to that of the current correlation. This correlation was established for a single array of plate finned elliptical tubes having axis ratio of 0.65. While, in the current study, plain elliptical tubes with axis ratio of 0.3 were used. Accordingly, it was expected to see better performance from the results in the current study. However, the current proposed correlation from is in satisfactory agreement with that of Bordalo and Saboya (1999).

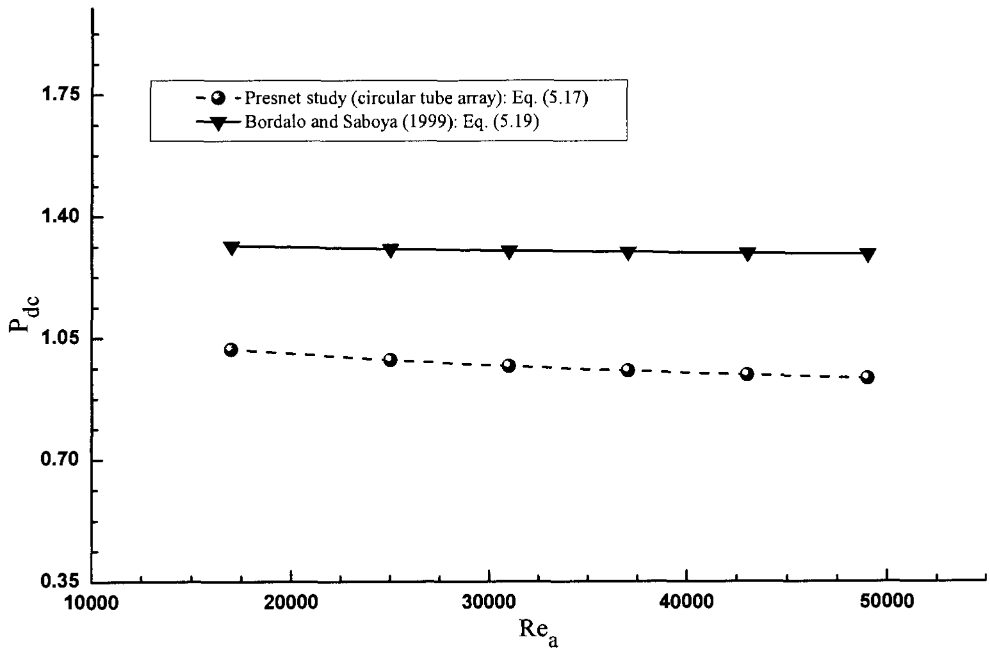

Figure 5.12 Comparison of $P_{dc} - Re_a$ correlation for the circular tube array with other results from the literature

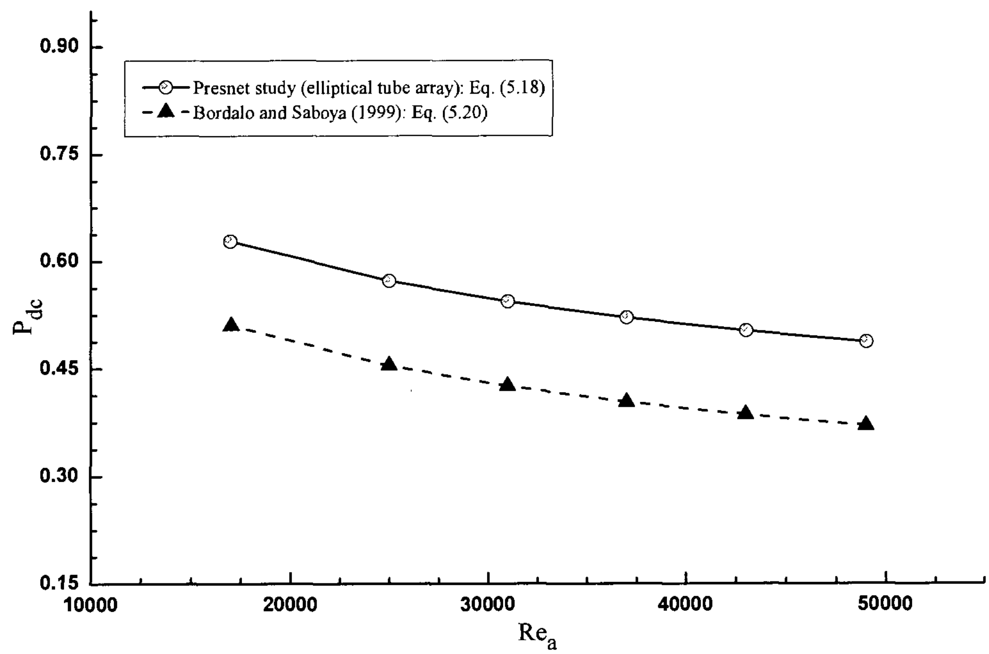

Figure 5.13 Comparison of $P_{dc} - Re_a$ correlation for the elliptical tube array with other results from the literature

5.5 Effect of Reynolds Number on Heat Transfer for the Water Flow

In this section, the heat transfer between the hot water flowing in the inside part of the tube and the air moving on the external surface is described. The variation of the water flow average Nusselt number with respect to Reynolds number was investigated. The water flow Reynolds and Nusselt numbers were calculated as illustrated in sections 4.4.1 and 4.4.2, respectively. A number of experiments were conducted on both circular and elliptical tube arrays. The experimental results are reported below.

The variations of the water flow Nusselt with Reynolds number for the circular and elliptical tube array are shown below in figures 5.14 and 5.15. The hot water and the cold air streams were forced to flow under similar conditions for both arrays. The water flow Reynolds number was varied in five steps from 900 to 9500. While, the air flow rate was ranged form 0.29 to 0.82 kg/s and 0.36 to 1.04 kg/s for the circular and elliptical tube arrays, respectively. Based on Eq. (4.12), six equations relate the variations of Nu_w on Re_w were obtained. The results are presented in table 5.2 below.

As seen in the figures below, the trend of Nu_w variation with respect to Re_w is similar for both arrays. The results show that Nu_w increases as Re_w increases in a power law form for the whole range covered in this study. This expected since at low values of Re_w, the viscosity plays a major role in forming the velocity boundary layer. The viscosity tends to slow the fluid down and thus increasing the velocity boundary layer thickness. Since the fluid velocity strongly affects the shape of the thermal boundary layer, the rate of heat convection decreases as Re_w decreases. It was also observed that for a fixed air flow rate, mainly Re_w influences the change in Nu_w. This due to high thermal resistance exerted at the air side.

Table 5.3 Nu_w as a function of Re_w at different air flow rate for the circular and elliptical tube arrays

m_a [kg/s]	Circular tube array	R^2	m_a [kg/s]	Elliptical tube array	R^2
0.29	$Nu_w = 0.981\ Re_w^{0.270}$	0.96	0.36	$Nu_w = 1.351\ Re_w^{0.231}$	0.97
0.43	$Nu_w = 1.056\ Re_w^{0.262}$	0.97	0.54	$Nu_w = 1.152\ Re_w^{0.253}$	0.96
0.52	$Nu_w = 1.086\ Re_w^{0.257}$	0.98	0.66	$Nu_w = 1.236\ Re_w^{0.244}$	0.96
0.64	$Nu_w = 1.290\ Re_w^{0.252}$	0.96	0.8	$Nu_w = 1.156\ Re_w^{0.251}$	0.99
0.73	$Nu_w = 1.152\ Re_w^{0.250}$	0.98	0.91	$Nu_w = 1.302\ Re_w^{0.239}$	0.95
0.82	$Nu_w = 1.056\ Re_w^{0.262}$	0.97	1.04	$Nu_w = 1.192\ Re_w^{0.249}$	0.96

From the results obtained in table 5.3 one overall correlation to predict the Nu_w variation with Re_w for the inner flow of water was established in the form of Eq. (4.12) as in Eq. (5.21). This correlation is applicable for the flow in both circular and elliptical tube arrays.

$$Nu_w = 1.144\ Re_w^{0.252} \qquad , R^2 = 0.97 \tag{5.21}$$

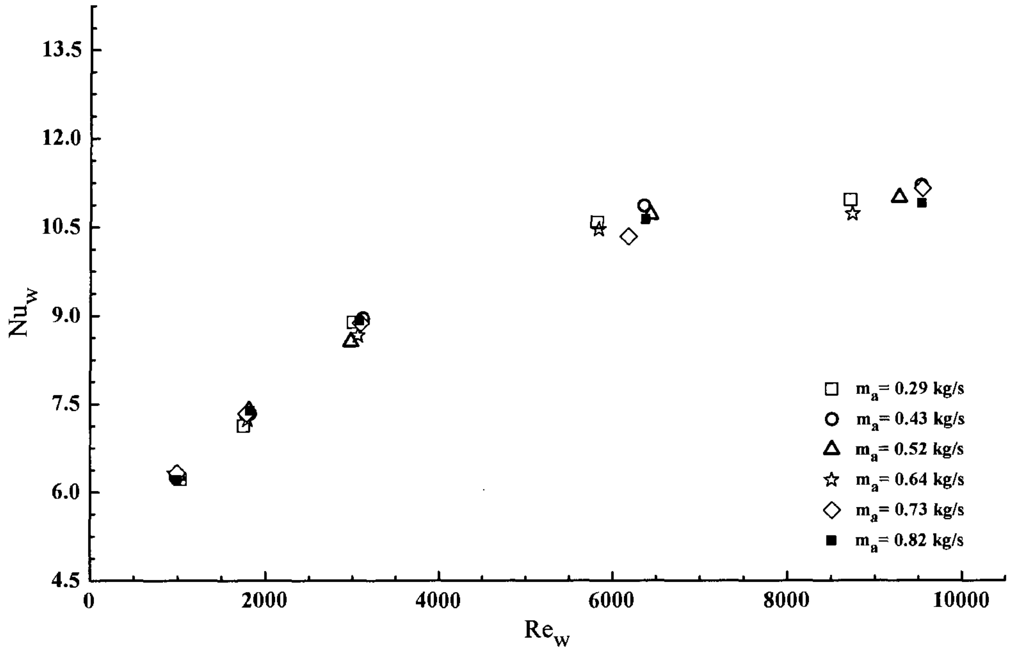

Figure 5.14 Nu_w variations with Re_w for different air flow rate for the case of the circular tube array

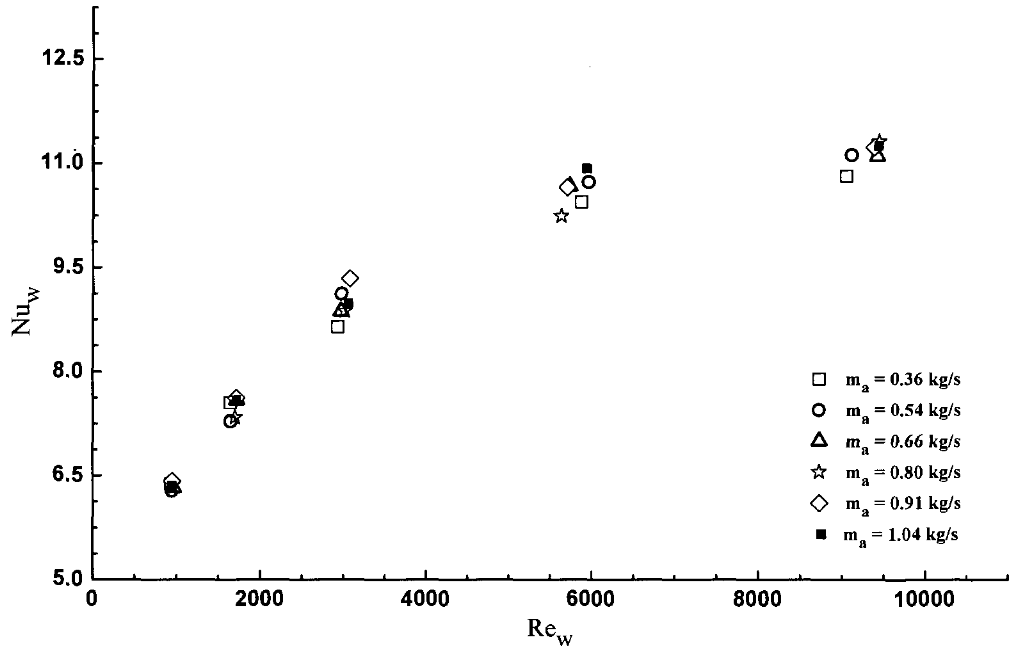

Figure 5.15 Nu_w variations with Re_w for different air flow rate for the case of the elliptical tube array

5.6 Comparison of the Water Flow Heat Transfer Results with the Available Results from the Literature

The present study overall Nu_w - Re_w are plotted in figure 5.16 below with other results from previous studies. One correlation found that proposed by Sieder and Tate (1936) for laminar flow inside a circular tube at isothermal surface boundary condition as in Eq. (5.16).

$$Nu_w = 1.86 \underbrace{(Re_w\, Pr_w)^{1/3} (L / D_{h_i})^{-1/3} (\mu_s / \mu_w)^{0.14}}_{X} \qquad (5.22)$$

This equation for $0.48 \le Pr_w \le 16700$, where μ_s is evaluated at the surface temperature, and L is total length of the tube. Whitaker (1972) suggested that the above correlation to be used for $x \ge 2$, which is the case in the present study. Within small variation in Pr_w in the present study, and introducing the circular tube inner diameter, D_i, and other parameters from the current study, the above correlation was simplified to take the following form

$$Nu_w = 0.596\, Re_w^{0.333} \qquad \text{(for } 900 \le Re_w \le 9500\text{)} \qquad (5.23)$$

Another correlation proposed by Gielinski (1976) for turbulent flow in the form of

$$Nu_w = \frac{(f / 2)(Re_w - 1000)\, Pr_w}{1 + 12.7 (f/2)^{1/2} (Pr_w^{\ 2/3} - 1)} \qquad (5.24)$$

where f is the pipe friction factor evaluated from Eq. (5.19) as recommended by Sadik and Hongtan (2002):

$$f = (1.58 \ln Re_w - 3.28)^{-2} \qquad (5.25)$$

Under the conditions considered in the present study, Eq. (5.18) was reduced to

$$Nu_w = 0.0048\, Re_w^{1.042} \qquad (900 \le Re_w \le 9500) \qquad (5.26)$$

Figure 5.16 shows that the current proposed Nu_w - Re_w agreed will the results obtained by Sieder and Tate (1936). At low Reynolds number the current study estimated slightly higher heat transfer than the proposed correlation of Sieder and Tate (1936). As the Reynolds number increases, however, the current results predict to some extent lower heat transfer rate. In the contrary, the current obtained results did not agree with that of Gnielinski. Gnielinski's correlation over predicted the heat transfer based on the present study parameters. This may attributed to fact that this correlation was established to for turbulence flow. For turbulence flow, high Reynolds number, the flow is highly disordered which results in more mixing to the flow, therefore, higher heat transfer as relative to low Reynolds number.

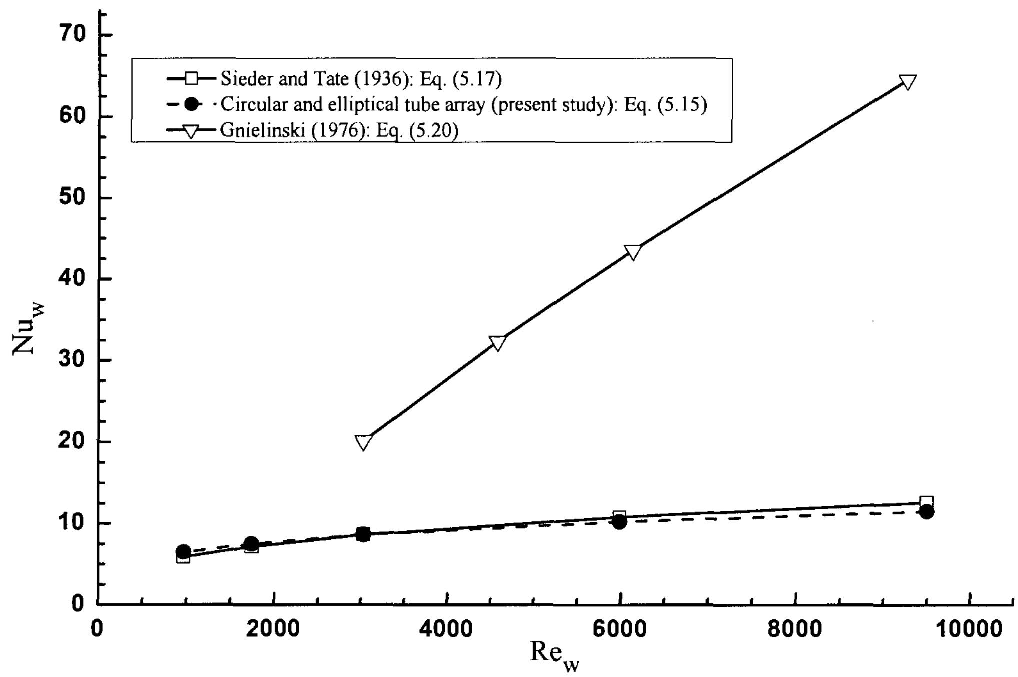

Figure 5.16 Comparison of present overall Nu_w vs Re_w with previous work

5.7 Uncertainties in the Results

The uncertainties associated with the temperature, velocity, pressure, and flow rate measurements propagated into the final results. It was found that the uncertainties associated with the final results at the air side not to exceed 5.6 %, 14.5 %, 19.4 %, and 19.6 % for Reynolds number, pressure drop coefficient, Nusselt number, and Stanton number, respectively. For the water side, the uncertainties associated with Reynolds number and Nusselt number were within 5.5 % and 19.8 % respectively. Sample of the uncertainty analysis procedure is explained in Appendix A.

CHAPTER 6
CONCLUSIONS AND RECOMMENDATIONS

Experimental study was carried out to investigate the force convection heat transfer between air and water in cross flow via circular and elliptical tube arrays. Cold air was forced to flow over the external surface of the tubes and exchange heat with the hot water flowing in the inside part. The experiments were conducted in close loop thermal wind tunnel. The same thermal and flow conditions were applied on both tube arrays. The air and water inlet temperature were maintained constant. The water flow rate was varied for both arrays from 0.01 to 0.11 kg/s. The air flow Reynolds number was varied in six steps from 17000 to 49000. Conclusions drawn from this study and recommendations for future work are summarized below.

6.1 Conclusions

6.1.1 Air Flow Results

Investigating the air flow heat transfer was the main objective of the current study. The relation between the air flow velocity and the heat transfer was established in dimensionless forms for Re_a ranging from 17000 to 49000. The pressure drop features for the air flow was also observed. Conclusions from the experimental results are as follows

- The study showed that mainly the air flow Reynolds number controls the heat transfer mechanism. It was found out that the effect of the water flow rate on the air flow heat transfer is insignificant. This is because of the high thermal resistance at the air side.

- The heat transfer was correlated with Reynolds number and the results were shown in the dimensionless form of Nu_a and St_a as functions of Re_a. The results indicated that Nu_a increases as Re_a increases in a power law relationship. In the contrary, St_a was found to decrease as Re_a increases following an inverse power law form. For the circular tube, the overall correlations were found as follows

  $$Nu_a = 0.162\ Re_a^{0.596}$$

  $$St_a = 0.241\ Re_a^{-0.412}$$

  and for the elliptical tube array the correlation were

  $$Nu_a = 0.288\ Re_a^{0.592}$$

  $$St_a = 0.334\ Re_a^{-0.392}$$

- The variation of the non dimensional pressure drop coefficient, P_{dc}, for the air flow with Reynolds number was observed. It was found that P_{dc}, varies with Re_a in an inverse power law form. A pressure drop correlation for the circular and elliptical tube arrays were proposed as

  $$P_{dc} = 2.216\ Re_a^{-0.080}$$

and for the elliptical tube array the correlation was

  $$P_{dc} = 6.508\ Re_a^{-0.240}$$

- It was concluded that utilizing the elliptical tubes not only minimizes the thermal resistance, but also minimizes the flow resistance. The present study revealed that by using the elliptical tube array 70 % enhancement in the heat transfer and 79 % reduction in the pressure drop as relative to the circular one were achieved.

- The air flow heat transfer and pressure drop results were compared with other results from the literature. The current results were found in satisfactory agreement with those of other studies.

6.1.2 Water Flow Results

Heat transfer for the water flow was also studied and conclusions from the experimental results are given below.

- It was shown that effect of Reynolds number on the heat transfer at the water side is similar to that at the air side. It was found that the influence of the air flow rate on the water side is negligible. The heat transfer features at the water flow is mainly dominated by the change in water flow Reynolds number. This is again, because of the high thermal resistance at the air side.
- The variation of Nu_w with Re_w was observed for Re_w ranging from 900 to 9500. An overall combined correlation applicable for the water flow inside the circular and elliptical tube arrays was established. The correlation was in term of Nu_w as functions of Re_w. The results showed that Nu_w increases as Re_w increases in a power law form as follows

  $$Nu_w = 1.144\ Re_w^{0.252}$$

- The heat transfer results were compared with others from the literature. It was found that the present results have reasonable agreements with that of other studies.

6.2 Recommendations

In the current study heat transfer and pressure drop characteristics of single in line circular and elliptical arrays were investigated under fixed geometrical and operating conditions. Therefore, further studies should include:

- Comparison of heat transfer results and pressure drop of the circular and elliptical tube arrays under similar operating conditions with different geometrical parameters. For instance:
  - Introducing fins at the air side for the current arrays.
  - Changing the tube arrangements to the staggered configurations.
  - Changing the diameter of the circular tube and the minor and major axes lengths of the elliptical tubes with the same axis ratio considered in the current study (0.3).
  - Investigate the tube to tube spacing effect.
  - Studying the influence of the number of tube rows.
- Numerical studies should be carried out for the same parameters and operating conditions.

REFERENCES

Badr, H. M. 1998. Forced convection from a straight elliptical tube. Heat and Mass Transfer , Vol. 34, pp. 229-236.

Brauer, H. 1964. Compact heat exchangers. J. Chem. Process Eng. pp. 451-460.

Bordalo, S. N. and Saboya F. E. M. 1999. Pressure Drop Coefficients for Elliptic and Circular Sections in One, Two and Three-Row Arrangements of Plate Fin and Tube Heat Exchangers. Journal of the Brazilian Society of Mechanical Sciences, Vol. 21, n. 4, pp. 600-610.

Buyruk, E. 1999. Heat transfer and flow structures around circular cylinders in cross-flow. Tr. J. of Engineering and Environmental Science, Vol. 23, pp. 299-315.

Castiglia, D., Balabani, S., Papadakis, G. and Yianneskis, M. 2001. An experimental and numerical study of the flow past elliptic cylinder arrays. Proceedings of the Institution of Mechanical Engineers, Vol. 215(C), pp. 1287-1301.

Çengel, Y. A. 2007. Heat Transfer – a practical approach. New York: McGraw-Hill Companies, Inc.

Gaddis, E. S. and Gnielinski, V. 1985. Pressure drop in cross flow across tube bundles. International Journal of Chemical Engineering, Vol. 25, No.1, pp. 1-15.

Gaddis, E. S. and Gnielinski, V. 1997. Pressure drop in cross flow across tube bundles. International Journal of Chemical Engineering, Vol. 25, No.1, pp. 1-15.

Gnielinski, V. 1976. New equations for heat and mass transfer in turbulent pipe and channel flow. International Journal of Chemical Engineering, Vol.16, No.2, pp. 359-368.

Gnielinski, V. 1979. Equations for calculating heat transfer in single tube rows and banks of tubes in transverse flow. International Journal of Chemical Engineering, Vol.19, No.3, pp. 380-391.

Harris, D. K. and Goldschmidt, V. W. 2002. Measurement of the overall heat transfer for combustion gases confined within elliptical tube heat exchangers. Experimental Thermal and Fluid Science, Vol. 26, pp. 33-37.

Hasan, A. and Sirén, K. 2004. Performance investigation of plain circular and oval tube evaporatively cooled heat exchangers. Applied Thermal Engineering, Vol. 24, pp. 777-790.

Horvat, A., Leskovar, M. and Mavko, B. 2006. Comparison of heat transfer conditions in tube bundle cross-flow for different tube shapes. International Journal of Heat and Mass Transfer, Vol. 49, pp. 1027-1038.

Ibrahim, T. A. and Gomma, A. Thermal performance criteria of elliptic tube bundle in cross flow. International Journal of Thermal Sciences (2009), doi:10.1016/j.ijthermalsci.2009.03.011

Incropera, F. P. and DeWitt, D. P. 2002. Fundamentals of Heat and Mass Transfer. 5th ed. New York: John Wiley & Sons, Inc.

Khan, M. G., Fartaj, A. and Ting, D. S-K. 2005. Study of cross-flow cooling and heating of air via an elliptical tube array. ASHRAE Transaction, Vol. 111 Part 1, pp. 423-433.

Kline, S. J. 1985. The purposes of uncertainty analysis. Journal of Fluids Engineering, Transactions of the ASME, Vol. 107, pp. 153 – 160.

Kline, S. J. and McClintock, F. A. 1953. Describing uncertainties in single sample experiments. Mechanical Engineering, Vol. 75, pp. 3-8.

Mainardes, R. L. S., Matos, R. S. and Vargas, J. V. C. 2007. Optimally staggered finned circular and elliptic tubes in turbulent forced convection. Jornal of Heat Transfer, Transaction of the ASME, Vol. 129, pp. 674-677.

Matos, R. S., Vargas, J. V. C., Laursen, T. A. and Saboya, F. E. 2001. Optimization study and heat transfer comparison of staggered circular and elliptic tubes in force convection. Journal of Heat and Mass Transfer, Vol. 44, pp. 3953-3961.

Merekr, G. P. and Hanke, H. 1986. Heat transfer and pressure drop on the shell-side of tube-banks having oval-shaped tubes. International Journal of Heat and Mass Transfer, Vol. 29, No. 12, pp. 1903-1909.

Moffat, R. J. 1985. Using uncertainty analysis in the planning of an experiment. Journal of Fluids Engineering, Transactions of the ASME, Vol. 107, pp. 173 – 178.

Muson, B. R. and Young, D. 2002. Fundamentals of Fluid Mechanics. 4th ed., John Wiley & Sons, Inc.

Nada, S. A., El-batsh, H. and Moawed, M. 2007. Heat transfer and fluid flow around semi-circular tube in cross flow at different orientations. Heat Mass Transfer, Vol. 43, pp. 1157-1169.

Nishiyama, H., Ota, T. and Matsuno, t. 1988. Heat transfer and flow around elliptic cylinders in tandem arrangement. JASME International Journal, Series II, Vol. 31, No. 3, pp. 410-419.

Ota, T., Nishiyama, H. and Taoka, Y. 1987. Flow around an elliptical cylinder in the critical Reynolds number regime. Journal of Fluids Engineering, Trans. ASME, Vol. 109, pp. 149-155.

Rahman, M. M., Salminen, E., and Siikonen, T. 2001. Heat transfer from circular and elliptic cylinders in cross flow. 4th International Conference on Mechanical Engineering, Bangladesh University of Engineering and Technology, Dhaka, Bangladesh, Vol. 2, pp. 203-207.

Rocha, L. A. O., Saboya, F. E. M. and Vrgas, J. V. C. 1997. A comparative study of elliptical and circular sections in one and two row tubes and plate fin heat exchangers. International Journal of Heat and Fluid Flow, Vol. 18, No. 2, pp. 247-252.

Sadik, K. and Hongtan, L. 2002. Heat Exchangers: Selection, Rating, and Thermal Design. Florida: CRC Press LLC.

Shah, R. K. and Sehulić D. P. 2003. Fundamentals of Heat Exchanger Design. New Jersey: John Wiley & Sons, Inc.

Shah, R. K. and London, A. L. 1978. Laminar Forced Convection in Ducts. New York: Academic Press.

Wang, C.C. 2000. Recent progress on the air side performance of fin and tube heat exchangers. International Journal of Heat Exchangers, Vol. 1, pp. 49-76.

Whitaker, S. 1972. Forced convection heat transfer correlations for flow in pipes, past flat plates, single cylinders, single spheres, and flow in packed beds and tubes. AICHE J., Vol. 18, pp. 361-371.

Wilson, A. S. and Bassiouny, M. K. 2000. Modeling of heat transfer for flow across tube banks. Chemical Engineering Processing, Vol. 39, pp. 1-14.

Žukauskas, A. 1972. Heat transfer from tubes in cross flow in Advances in Heat Transfer, Edited by Hartnett, J. P. and Irvine, T. F. Jr, New York: Academic Press. Vol. 8, pp. 93-160.

Žukauskas, A. and Ulinskas, R. 1988. Heat Transfer in tube banks in cross flow. Washington: Hemisphere Publishing Corporation.

APPENDIX A
UNCERTAINTY ANALYSIS

The uncertainty associated with the measurements of the temperature, flow rate, pressure drop, fluid properties, and the dimensions of the tubes propagated into the final results. The method of estimating the uncertainty of Re, P_{dc}, Nu, and St as the final results was performed based on the suggestions of Kline and McClintock (1953), Kline (1985), and Moffat (1985). Described below is a sample calculation of the uncertainty analysis based on a set of results obtained from the circular tube array.

A.1 Uncertainty in the Dimensions of the Tubes

The dimensions of the tubes were measured using a digital caliper with 0.0254 mm accuracy, and 0.0127 mm resolution. From these specifications, the total error associated with the digital caliper was included as a bias error, B. It was estimated as follows

$$B = \sqrt{(0.0254)^2 + (0.0127)^2} = 0.0284 \text{ mm}$$

A repeatability error associated with each of the ten individual repeated measurements of D_i, D_o, L and S was also included as a precision error, P. From the student distribution at 95 % confidence interval and the standard deviation of the mean, the precision error was estimated for each of tube dimension. Table A.1 below show the tube dimensions measurements data and the total errors associated the measurements.

Table A.1 Tube dimensions data

N	**Dimension [mm]**			
$t_{N-1,95} = 2.262$	**S**	D_i	D_o	**L**
1	6.20	20.57	22.31	304.31
2	6.12	20.54	22.29	304.60
3	6.00	20.63	22.22	303.92
4	6.32	20.53	22.20	304.21
5	6.11	20.54	22.24	304.53
6	6.10	20.62	22.28	303.76
7	6.40	20.62	22.15	302.87
8	6.33	20.58	22.09	302.22
9	6.23	20.54	22.19	304.01
10	6.42	20.53	22.16	303.93
Mean Value	6.22	20.57	22.21	303.84
S_{dm}	0.0447	0.0127	0.0219	0.2364
P	0.1011	0.0288	0.0496	0.5348
B	0.0284	0.0284	0.0284	0.0284
U	0.1050	0.0405	0.0571	0.5355

A.1.1 Uncertainty Associated with the Total Length of the Tube

The total length of the tube was calculated as

$$L_t = 10\,L = 3.04\text{ m}$$

The uncertainty in L_t was calculated as

$$U_{L_t} = \frac{\partial_{U_{L_t}}}{\partial L} U_L,$$

where $\quad \frac{\partial_{U_{L_t}}}{\partial L} = 10$, and U_L was taken from table A.1.

Thus $U_{L_t} = \pm\ 53.55 \times 10^{-4}$ m.

A.1.2 Uncertainty Associated with the Inner Surface Area of the Tube

The total inner surface area was calculated as

$$A_{S_i} = \pi\ D_i\ L_t$$

The uncertainty in A_{S_i} was calculated as follows

$$U_{A_{S_i}} = \sqrt{\left(\frac{\partial A_{S_i}}{\partial D_i} U_{D_i}\right)^2 + \left(\frac{\partial A_{S_i}}{\partial_{L_t}} U_{L_t}\right)^2},$$

where $\quad \frac{\partial A_{S_i}}{\partial D_i} = \pi L_t$ and U_{D_i} was taken from table A.1, and

$\frac{\partial A_{S_i}}{\partial_{L_t}} = \pi D_i$ and $U_{L_t} = \pm\ 53.55 \times 10^{-4}$ m.

Thus $\quad U_{A_{S_i}} = \pm\ 5.19 \times 10^{-4}$ m^2.

A.1.3 Uncertainty Associated with the Outer Surface Area of the Tube

The total outer surface area was calculated as

$$A_{S_o} = \pi\ D_o\ L_t$$

The uncertainty in A_{S_i} was calculated as follows

$$U_{A_{S_o}} = \sqrt{\left(\frac{\partial A_{S_o}}{\partial D_o} U_{D_o}\right)^2 + \left(\frac{\partial A_{S_o}}{\partial_{L_t}} U_{L_t}\right)^2},$$

where $\frac{\partial A_{S_O}}{\partial D_o} = \pi L_t$ and U_{D_o} was taken from table A.1, and

$$\frac{\partial A_{S_O}}{\partial_{L_t}} = \pi D_o \text{ and } U_{L_t} = \pm\ 53.55 \times 10^{-4}\ \text{m}.$$

Thus $U_{A_{S_O}} = \pm\ 6.61 \times 10^{-4}\ \text{m}^2$.

A.1.4 Uncertainty Associated with the Inner Cross Section Area of the Tube

The inner surface area of the tube was calculated as

$$A_{w_i} = \frac{\pi}{4}\ D_i^2$$

The uncertainty in A_{S_i} was calculated as follows

$$U_{A_{w_i}} = \sqrt{\left(\frac{\partial A_{w_i}}{\partial D_i} U_{D_i}\right)^2},$$

where $\frac{\partial A_{w_i}}{\partial D_i} = \frac{\pi}{2} D_i$ and U_{D_i} was taken from table A.1.

Thus $U_{A_{w_i}} = \pm\ 1.31 \times 10^{-6}\ \text{m}^2$.

A.2 Uncertainty Associated with the Measurements of Temperature

Type T thermocouples were used in this study to measure the temperatures at different locations for the air and water flow. The thermocouples were connected to a data acquisition system. A complete system calibration was performed. Readings from the data acquisition system were calibrated against readings from Dry Block temperature calibrator. Errors associated with the temperature measurements were mainly due to the calibration. Therefore, a value of $\pm$ 0.1 °C was estimated as the total uncertainty in any of the temperature measurements.

A.3 Uncertainty Associated with the Properties of Air

Uncertainty Associated with the Density of Air

The air density was evaluated at the inlet temperature for calculating the air velocity at the inlet. For calculating Reynolds number and the pressure drop coefficient at the air side, it was evaluated at the film temperature. For air as an ideal gas the density was calculated as follows

$$\rho_a = \frac{P_{ab}}{R\,T}$$

For the inlet conditions where $T_i = 15.79$ °C and $P_{ab} = 100.07$ Pa , the uncertainty in ρ_{a_i} was calculated as

$$U_{\rho_{a_i}} = \sqrt{\left(\frac{\partial \rho_{a_i}}{\partial P_{ab}} U_{P_{ab}}\right)^2 + \left(\frac{\partial \rho_{a_i}}{\partial_{T_{a_i}}} U_{T_{a_i}}\right)^2},$$

where $\frac{\partial \rho_{a_i}}{\partial P_{ab}} = \frac{1}{R\,T_i}$ and, and $U_{P_{ab}} = \pm$ 500 Pa

$$\frac{\partial \rho_a}{\partial_{T_i}} = -\frac{P_{ab}}{R\,T_i^2}, \text{ and } U_{T_{a_i}} = \pm\ 0.1\ °C.$$

Thus $U_{\rho_{a_i}} = \pm$ 0.006 kg/m^3.

At the film conditions where $T_{a_f} = 23.31$ °C and $P_{ab} = 100.07$ Pa , the uncertainty in ρ_{a_f} was estimated to be the same as that at the inlet conditions.

Uncertainty Associated with the Dynamic Viscosity of Air

Considering the film conditions of $T_{f_{min}} = 24.50\ ^\circ C$ and $T_{f_{min}} = 26.53\ ^\circ C$, μ_a was 1.847×10^{-5} kg/m s and 1.856×10^{-5} kg/m s, respectively. The uncertainty associated with the dynamic viscosity of air at the film conditions was calculated as follows

$$U_{\mu_{a_f}} = \pm\frac{1}{2}\left(\mu_{a_{max}} - \mu_{a_{min}}\right)$$

$$U_{\mu_{a_f}} = \pm\ 4.5\times10^{-8}\ \text{kg/m s}$$

Uncertainty Associated with the Thermal Conductivity of Air

At the film conditions where $T_{f_{min}} = 24.50\ ^\circ C$ and $T_{f_{min}} = 26.53\ ^\circ C$, k_a was 0.02547 W/m°C and 0.02562 W/m°C , respectively. The uncertainty associated with the thermal conductivity of air at the film conditions was calculated as follows

$$U_{k_{a_f}} = \pm\frac{1}{2}\left(k_{a_{max}} - k_{a_{min}}\right)$$

$$U_{k_{a_f}} = \pm\ 7.5\times10^{-5}\ \text{W/m}^\circ\text{C}$$

A.4 Uncertainty Associated with the Properties of Water

The uncertainties associated with the water properties were estimated considering the average conditions of $T_{w_{b_{min}}} = 34.10\ ^\circ C$ and $T_{w_{b_{max}}} = 38.57\ ^\circ C$ as follows

Uncertainty Associated with the Density of Water

$$U_{\rho_w} = \pm\ \frac{1}{2}\left(\rho_{w_{max}} - \rho_{w_{min}}\right)$$

$$U_{\rho_w} = \pm\ 0.9\ \text{kg/m}^3$$

Uncertainty Associated with the Dynamic Viscosity of Water

$$U_{\mu_w} = \pm\ \frac{1}{2}\left(\mu_{w_{max}} - \mu_{w_{min}}\right)$$

$$U_{\mu_w} = \pm\ 3.1\times10^{-5}\ \text{kg/m s}$$

Uncertainty Associated with the Thermal Conductivity of Water

$$U_{k_w} = \pm\frac{1}{2}\left(k_{w_{max}} - k_{w_{min}}\right)$$

$$U_{k_w} = \pm\ 0.0035\text{W/m°C}$$

A.5 Uncertainty Associated with the Air Flow Velocity at the Inlet

The air flow velocity was measured using a Pitot static. From Eq. (3.1) the velocity was defined as

$$V_{a_i} = \sqrt{\frac{2\ P_{dyn}}{\rho_{a_i}}}$$

For $\rho_{a_i} = 1.207$ kg/m^3 and $P_{dyn} = 33.05$ Pa , the uncertainty in V_{a_i} was calculated as

$$U_{V_{a_i}} = \sqrt{\left(\frac{\partial V_{a_i}}{\partial P_{dyn}} U_{P_{dyn}}\right)^2 + \left(\frac{\partial V_{a_i}}{\partial \rho_{a_i}} U_{\rho_{a_i}}\right)^2},$$

where $\dfrac{\partial V_{a_i}}{\partial P_{dyn}} = \dfrac{1}{\sqrt{2\ P_{dyn}\ \rho_{a_i}}}$ and $U_{P_{dyn}} = \pm\ 0.44$ Pa , and

$$\frac{\partial V_{a_i}}{\partial \rho_{a_i}} = -\sqrt{\frac{P_{dyn}}{2\rho_{a_i}^3}}\ \text{and}\ U_{\rho_{a_i}} = \pm\ 0.006\ \text{kg/m}^3.$$

Thus $U_{V_{a_i}} = \pm\ 0.0526$ m/s.

A.6 Uncertainty Associated with the Air Flow Velocity at the Minimum Cross Section

The velocity at the minimum cross section was calculated from Eq. (4.16) as

$$V_{a_{max}} = \frac{S + D_o}{S} V_a$$

For $V_a = 7.4$ m/s, $S = 0.0062$ m and $D_o = 0.0222$ m, the uncertainty in associated with $V_{a_{max}}$ was calculated as

$$U_{V_{a_{max}}} = \sqrt{\left(\frac{\partial V_{a_{max}}}{\partial V_a} U_{V_a}\right)^2 + \left(\frac{\partial V_{a_{max}}}{\partial D_o} U_{D_o}\right)^2 + \left(\frac{\partial V_{a_{max}}}{\partial S} U_S\right)^2},$$

where $\frac{\partial V_{a_{max}}}{\partial V_a} = \frac{S + D_o}{S}$ and $U_{V_a} = \pm\ 0.0526$ m/s,

$\frac{\partial V_{a_{max}}}{\partial D_o} = \frac{V_a}{S}$ and $U_{D_o} = \pm\ 5.71 \times 10^{-5}$ m, and

$\frac{\partial V_{a_{max}}}{\partial S} = -\frac{D_o}{S^2} V_a$ and $U_S = \pm\ 1.05 \times 10^{-4}$ m.

Thus $U_{V_{a_{max}}} = \pm\ 0.5138$ m/s.

A.7 Uncertainty Associated with the Water Flow Velocity at the Inlet

The water velocity was calculated from Eq. (4.19) as follows

$$V_{w_i} = \frac{FR_{w_i}}{A_i}$$

At the inlet conditions where $\rho_{w_i} = FR_{w_i} = 7.1 \times 10^{-5}$ m^3/s and $A_i = 3.32 \times 10^{-4}$ m^2, the uncertainty in V_{w_i} was calculated as

$$U_{V_{w_i}} = \sqrt{\left(\frac{\partial V_{w_i}}{\partial A_{w_i}} U_{A_{w_i}}\right)^2 + \left(\frac{\partial V_{w_i}}{\partial FR_{w_i}} U_{FR_{w_i}}\right)^2},$$

where $\frac{\partial V_{w_i}}{\partial A_{w_i}} = -\frac{FR_{w_i}}{A_{w_i}^2}$ and $U_{A_{w_i}} = \pm\ 1.31\times10^{-6}\ m^2$, and

$\frac{\partial V_w}{\partial FR_{w_i}} = \frac{1}{A_{w_i}}$ and $U_{FR_{w_i}} = \pm\ 3.1\times10^{-6}\ m^3/s$.

Thus $U_{V_{w_i}} = \pm\ 0.001$ m/s.

A.8 Uncertainty Associated with the Air Flow Rate

The air flow rate was calculated from Eq. (4.24) as

$$m_a = \rho_{a_i}\ V_{a_i}\ A_{a_i}$$

For $V_a = 7.4$ m/s, $\rho_{a_i} = 1.207$ kg/m^3 and $A_{i_o} = 0.0929$ m^2, the uncertainty associated with m_a was calculated as

$$U_{m_a} = \sqrt{\left(\frac{\partial m_a}{\partial \rho_{a_i}} U_{\rho_{a_i}}\right)^2 + \left(\frac{\partial m_a}{\partial V_{a_i}} U_{V_{a_i}}\right)^2},$$

where $\frac{\partial m_a}{\partial \rho_{a_i}} = V_{a_i} A_{a_i}$ and $U_{\rho_{a_i}} = \pm\ 0.006$ kg/m^3, and

$\frac{\partial m_a}{\partial V_{a_i}} = \rho_{a_i}\ A_{a_i}$ and $U_{V_{a_i}} = \pm\ 0.0526$ m/s.

Thus $U_{m_a} = \pm\ 0.01$ kg/s.

A.9 Uncertainty Associated with the Water Flow Rate

The Water flow rate as defined in Eq. (4.25) was calculated as

$$m_w = \rho_{w_i}\ FR_{w_i}$$

For $\rho_{w_i} = 993.1$ kg/m^3 and $FR_{w_i} = 7.1\times10^{-5}$ m^3/s, the uncertainty associated with m_w was calculated as

$$U_{m_w} = \sqrt{\left(\frac{\partial m_w}{\partial \rho_{w_i}} U_{\rho_{w_i}}\right)^2 + \left(\frac{\partial m_w}{\partial FR_{w_i}} U_{FR_{w_i}}\right)^2},$$

where $\dfrac{\partial m_w}{\partial \rho_{w_i}} = FR_{w_i}$, and $U_{\rho_w} = \pm\ 0.9$ kg/m^3, and

$\dfrac{\partial m_w}{\partial FR_{w_i}} = \rho_{w_i}$, and $U_{FR_{w_i}} = \pm\ 3.1\times10^{-6}$ m^3/s.

Thus $U_{m_w} = \pm\ 0.003$ kg/s.

A.10 Uncertainty Associated with the Heat Transfer Rate at the Air Side

The heat transfer rate for the air side was calculated from Eq. (4.21) as

$$Q_a = m_a c_{p_a}(T_{a_i} - T_{a_e})$$

For the air conditions where $m_a = 0.82$ kg/s, $c_{p_a} = 1007$ J/kg °C, $T_{a_i} = 15.79$ °C and $T_{a_i} = 16.28$ °C, the uncertainty in Q_a was calculated as

$$U_{Q_a} = \sqrt{\left(\frac{\partial Q_a}{\partial m_a} U_{m_a}\right)^2 + \left(\frac{\partial Q_a}{\partial T_{a_i}} U_{T_{a_i}}\right)^2 + \left(\frac{\partial Q_a}{\partial T_{a_e}} U_{T_{a_e}}\right)^2},$$

where $\dfrac{\partial Q_a}{\partial m_a} = c_{p_a}(T_{a_e} - T_{a_i})$ and $U_{m_a} = \pm\ 0.01$ kg/s,

$\dfrac{\partial Q_a}{\partial T_{a_i}} = -m_a c_{p_a}$ and $U_{T_{a_i}} = \pm\ 0.1$ °C, and

$$\frac{\partial Q_a}{\partial T_{a_e}} = m_a c_{p_a} \text{ and } U_{T_{a_e}} = \pm\, 0.1\ ^\circ\text{C}.$$

Thus $U_{Q_a} = \pm\, 116.88$ W.

A.11 Uncertainty Associated with the Heat Transfer Rate at the Water Side

The heat transfer rate for the water side was calculated from Eq. (4.20) as

$$Q_w = m_w c_{p_w} (T_{w_i} - T_{w_e})$$

For the water conditions where $m_w = 0.07$ kg/s, $c_{p_a} = 4180$ J/kg °C, $T_{w_i} = 37.34$ °C and $T_{w_e} = 36.15$ °C, the uncertainty in Q_w was calculated as

$$U_{Q_w} = \sqrt{\left(\frac{\partial Q_w}{\partial m_w} U_{m_w}\right)^2 + \left(\frac{\partial Q_w}{\partial T_{w_i}} U_{T_{w_i}}\right)^2 + \left(\frac{\partial Q_w}{\partial T_{w_e}} U_{T_{w_e}}\right)^2},$$

where $\frac{\partial Q_w}{\partial m_w} = c_{p_w} (T_{w_i} - T_{w_e})$ and $U_{m_w} = \pm\, 0.003$ kg/s,

$$\frac{\partial Q_w}{\partial T_{w_i}} = m_w c_{p_w} \text{ and } U_{T_{w_i}} = \pm\, 0.1\ ^\circ\text{C, and}$$

$$\frac{\partial Q_w}{\partial T_{w_e}} = -m_w c_{p_w} \text{ and } U_{T_{w_e}} = \pm\, 0.1\ ^\circ\text{C}.$$

Thus $U_{Q_w} = \pm\, 43.99$ W.

A.12 Uncertainty Associated with the Average Heat Transfer Rate

The average heat transfer rate was calculated from Eq. (4.22) as follows

$$Q = \frac{Q_w + Q_a}{2}$$

For $Q_a = 404.6$ W, $Q_w = 348.2$ W and $Q = 376.4$ W, the uncertainty in Q was calculated as

$$U_Q = \sqrt{\left(\frac{\partial Q}{\partial Q_a} U_{Q_a}\right)^2 + \left(\frac{\partial Q}{\partial Q_w} U Q_w\right)^2},$$

where $\frac{\partial Q}{\partial Q_a} = \frac{1}{2}$ and $U_{Q_a} = \pm\ 116.88$ W, and

$\frac{\partial Q}{\partial Q_w} = \frac{1}{2}$ and $U_{Q_w} = \pm\ 43.99$ W.

Thus $U_Q = \pm\ 62.44$ W.

A.13 Uncertainty Associated with the Heat Transfer Coefficient at the Air Side

The average heat transfer coefficient for the air flow was estimated from Eq. (4.25) as follows

$$h_a = \frac{Q}{A_{s_o}(T_s - T_{a_i})}$$

For $Q = 376.4$ W, $A_{s_o} = 0.2119$ m^2, $T_s = 30.82$ °C and $T_{a_i} = 15.79$ °C, the uncertainty in h_a was calculated as

$$U_{h_a} = \sqrt{\left(\frac{\partial h_a}{\partial Q} U_Q\right)^2 + \left(\frac{\partial h_a}{\partial A_{s_o}} U_{A_{s_o}}\right)^2 + \left(\frac{\partial h_a}{\partial T_s} U_{T_s}\right)^2 + \left(\frac{\partial h_a}{\partial T_{a_i}} U_{T_{a_i}}\right)^2},$$

Where $\frac{\partial h_a}{\partial Q} = \frac{1}{A_{s_o}(T_s - T_{a_i})}$ and $U_Q = \pm\ 62.44$ W,

$\frac{\partial h_a}{\partial A_{s_o}} = -\frac{Q}{A_{s_o}^2(T_s - T_{a_i})}$ and $U_{A_{s_o}} = \pm\ 6.61 \times 10^{-4}$ m^2,

$$\frac{\partial h_a}{\partial T_s} = -\frac{Q}{A_{s_o}(T_s - T_{a_i})^2} \text{ and } U_{T_s} = \pm\ 0.1\ ^\circ C, \text{ and}$$

$$\frac{\partial h_a}{\partial T_{a_i}} = \frac{Q}{A_{s_o}(T_s - T_{a_i})^2} \text{ and } U_{T_{a_i}} = \pm\ 0.1\ ^\circ C.$$

Thus $U_{h_a} = \pm\ 19.64\ W/m^2\,^\circ C$.

A.14 Uncertainty Associated with the Nusselt Number at the Air Side

The Nusselt number at the air side was calculated from Eq. (4.26) as follows

$$Nu_a = \frac{h_a D_o}{k_a}$$

For $h_a =\ 118.18\ W/m^2\,^\circ C$, $D_o = 0.0222$ m, $k_{a_f} = 0.02538 W/m^\circ C$ and $Nu_a = 103.37$ the uncertainty associated with Nu_a was calculated as

$$U_{Nu_a} = \sqrt{\left(\frac{\partial U_{Nu_a}}{\partial h_a} U_{h_a}\right)^2 + \left(\frac{\partial U_{Nu_a}}{\partial D_o} U_{D_o}\right)^2 + \left(\frac{\partial U_{Nu_a}}{\partial k_{a_f}} U_{k_{af}}\right)^2},$$

where $$\frac{\partial U_{Nu_a}}{\partial h_a} = \frac{D_o}{k_{a_f}} \text{ and } U_{h_a} = \pm\ 19.64\ W/m^2\,^\circ C,$$

$$\frac{\partial U_{Nu_a}}{\partial D_o} = \frac{h_a}{k_{a_f}} \text{ and } U_{D_o} = \pm\ 5.71 \times 10^{-5} \text{ m, and}$$

$$\frac{\partial U_{Nu_a}}{\partial k_{a_f}} = -\frac{h_a D_o}{k_{a_f}^2} \text{ and } U_{k_{af}} = \pm\ 7.5 \times 10^{-5} W/m^\circ C.$$

Thus $U_{Nu_a} = \pm\ 17.18$ and

$$\frac{U_{Nu_a}}{Nu_a} = \pm\ 16.6\ \%.$$

A.15 Uncertainty Associated with the Stanton Number at the Air Side

The Stanton number at the air side was calculated from E. (4.28) as follows

$$\mathrm{St_a} = \frac{h_\mathrm{a}}{\rho_{\mathrm{a_f}} \mathrm{V_{a_{max}}} \mathrm{c_{p_a}}}$$

For h_a = 118.18 W/m^2°C, $\mathrm{V}_{\mathrm{a}_{max}}$ = 34.07 m/s, ρ_{a_f} = 1.177 kg/m^3, $\mathrm{c_{p_a}}$ =1007 J/kg °C

and $\mathrm{St_a} = 0.0029$, the uncertainty associated with $\mathrm{St_a}$ was calculated as

$$\mathrm{U_{St_a}} = \sqrt{\left(\frac{\partial \mathrm{U_{St_a}}}{\partial h_\mathrm{a}} \mathrm{U}_{h_\mathrm{a}}\right)^2 + \left(\frac{\partial \mathrm{U_{St_a}}}{\partial \rho_{\mathrm{a_f}}} \mathrm{U}\rho_{\mathrm{a}_f}\right)^2 + \left(\frac{\partial \mathrm{U_{St_a}}}{\partial \mathrm{V_{a_{max}}}} \mathrm{UV}_{\mathrm{a}_{max}}\right)^2},$$

where $\frac{\partial \mathrm{U_{St_a}}}{\partial h_\mathrm{a}} = \frac{1}{\rho_{\mathrm{a_f}} \mathrm{V_{a_{max}}} \mathrm{c_{p_a}}}$ and $\mathrm{U}_{h_\mathrm{a}} = \pm$ 19.64 W/m^2°C,

$$\frac{\partial \mathrm{U_{St_a}}}{\partial \rho_{\mathrm{a_f}}} = -\frac{h_\mathrm{a}}{\rho^2_{\mathrm{a_f}} \mathrm{V_{a_{max}}} \mathrm{c_{p_a}}}$$ and $\mathrm{U}_{\rho_{\mathrm{af}}} = \pm$ 0.006 kg/m^3, and

$$\frac{\partial \mathrm{U_{St_a}}}{\partial \mathrm{V_{a_{max}}}} = -\frac{h_\mathrm{a}}{\rho_{\mathrm{a_f}} \mathrm{V^2_{a_{max}}} \mathrm{c_{p_a}}}$$ and $\mathrm{U_{V_{a\,max}}} = \pm$ 0.5138 m/s.

Thus $\mathrm{U_{St_a}} = \pm\ 4.89 \pm 10^{-4}$ and

$$\frac{\mathrm{U_{St_a}}}{\mathrm{St_a}} = \pm\ 16.8\ \%.$$

A.16 Uncertainty Associated with the Heat Transfer Coefficient at the Water Side

The heat transfer coefficient for the water flow was estimated from Eq. (4.29) as follows

$$h_\mathrm{w} = \frac{Q}{\mathrm{A_{s_i}} (\mathrm{T_{w_b}} - \mathrm{T_s})}$$

For $Q = 376.4$ W, $A_{s_i} = 0.1963$ m^2, $T_s = 30.82$ °C and $T_{w_b} = 36.75$ °C, the uncertainty in h_w was calculated as

$$U_{h_w} = \sqrt{\left(\frac{\partial h_w}{\partial Q} U_Q\right)^2 + \left(\frac{\partial h_w}{\partial A_{s_i}} U_{A_{s_i}}\right)^2 + \left(\frac{\partial h_a}{\partial T_{w_b}} U_{T_{w_b}}\right)^2 + \left(\frac{\partial h_a}{\partial T_s} U_{T_s}\right)^2},$$

Where $\dfrac{\partial h_w}{\partial Q} = \dfrac{1}{A_{s_i}(T_{w_b} - T_s)}$ and $U_Q = \pm$ 62.44 W,

$\dfrac{\partial h_w}{\partial A_{s_i}} = -\dfrac{Q}{A_{s_i}^2(T_{w_b} - T_s)}$ and $U_{A_{s_i}} = \pm\ 5.19\times10^{-4}$ m^2,

$\dfrac{\partial h_w}{\partial T_s} = -\dfrac{Q}{A_{s_i}(T_{w_b} - T_s)^2}$ and $U_{T_s} = \pm$ 0.1 °C, and

$\dfrac{\partial h_w}{\partial T_s} = \dfrac{Q}{A_{s_i}(T_{w_b} - T_s)^2}$ and $U_{T_{w_b}} = \pm$ 0.1 °C.

Thus $U_{h_w} = \pm$ 54.20 W/m^2 °C.

A.17 Uncertainty Associated with the Nusselt Number at the Water Side

The Nusselt number at the water side was calculated from E. (4.30) as follows

$$Nu_w = \frac{h_w D_i}{k_w}$$

For $h_w =$ 323.35 W/m^2 °C, $D_i = 0.0206$ m, $k_{w_b} = \pm$ 0.625W/m°C and $Nu_w = 10.66$ the uncertainty associated with Nu_w was calculated as

$$U_{Nu_w} = \sqrt{\left(\frac{\partial U_{Nu_w}}{\partial h_w} U_{h_w}\right)^2 + \left(\frac{\partial U_{Nu_w}}{\partial D_i} U_{D_i}\right)^2 + \left(\frac{\partial U_{Nu_w}}{\partial k_{w_b}} U_{k_{w_b}}\right)^2},$$

where $$\frac{\partial U_{Nu_w}}{\partial h_w} = \frac{D_i}{k_{w_b}} \text{ and } U_{h_w} = \pm\ 54.20\ \text{W/m}^2\,{}^\circ\text{C},$$

$$\frac{\partial U_{Nu_w}}{\partial D_i} = \frac{h_w}{k_{w_b}} \text{ and } U_{D_i} = \pm\ 4.05\times10^{-5}\ \text{m, and}$$

$$\frac{\partial U_{Nu_w}}{\partial k_{w_b}} = -\frac{h_w D_i}{k_{w_b}^2} \text{ and } U_{k_{w_b}} = \pm\ 0.0035\,\text{W/m}^\circ\text{C}.$$

Thus $U_{Nu_w} = \pm\ 1.79$ and

$$\frac{U_{Nu_w}}{Nu_w} = \pm\ 16.8\ \%.$$

A.18 Uncertainty Associated with the Air Flow Reynolds Number

The air flow Reynolds number was calculated from Eq. (4.15) as

$$Re_a = \frac{\rho_{a_f} V_{a_{max}} D_o}{\mu_{a_f}}$$

For $V_{a_{max}} = 34.07$ m/s, $\rho_{a_f} = 1.177$ kg/m^3, $D_o = 0.0222$ m, $\mu_{a_f} = 1.841\times10^{-5}$ kg/m s and $Re_a = 48356$, the uncertainty in Re_a was calculated as follows

$$U_{Re_a} = \sqrt{\left(\frac{\partial U_{Re_a}}{\partial \rho_{a_f}} U_{\rho_{a_f}}\right)^2 + \left(\frac{\partial U_{Re_a}}{\partial V_{a_{max}}} U_{V_{a_{max}}}\right)^2 + \left(\frac{\partial U_{Re_a}}{\partial D_o} U_{D_o}\right)^2 + \left(\frac{\partial U_{Re_a}}{\partial \mu_{a_f}} U_{\mu_{a_f}}\right)^2},$$

where $$\frac{\partial U_{Re_a}}{\partial \rho_{a_f}} = \frac{V_{a_{max}} D_o}{\mu_{a_f}} \text{ and } U_{\rho_{a_f}} = \pm\ 0.006\ \text{kg/m}^3,$$

$$\frac{\partial U_{Re_a}}{\partial V_{a_{max}}} = \frac{\rho_{a_f} D_o}{\mu_{a_f}} \text{ and } U_{V_{a_{max}}} = \pm\ 0.5138\ \text{m/s},$$

$$\frac{\partial U_{Re_a}}{\partial D_o} = \frac{\rho_{a_f} V_{a_{max}}}{\mu_{a_f}} \text{ and } U_{D_o} = \pm\ 5.71\times10^{-5}\ \text{m, and}$$

$$\frac{\partial U_{Re_a}}{\partial \mu_{a_f}} = -\frac{\rho_{a_f}\, V_{a_{max}}\, D_o}{\mu_{a_f}^2} \text{ and } U_{\mu_{a_f}} = \pm\, 4.5\times10^{-8} \text{ kg/m s.}$$

Thus $U_{Re_a} = \pm\, 789$ and

$$\frac{U_{Re_a}}{Re_a} = \pm\, 1.63\ \%.$$

A.19 Uncertainty Associated with the Water Flow Reynolds Number

The water flow Reynolds number was calculated from Eq. (4.18) as

$$Re_w = \frac{\rho_{w_b} V_{w_i}\, D_i}{\mu_{w_b}}$$

For V_{w_i} = 0.214 m/s, ρ_{a_f} = 993.3 kg/m^3, D_i= 0.0206 m, μ_{w_b} = 0.697 × 10^{-3} kg/m s and

$Re_a = 6282$, the uncertainty in Re_a was calculated as follows

$$U_{Re_w} = \sqrt{\left(\frac{\partial U_{Re_w}}{\partial \rho_{w_b}} U_{\rho_{w_b}}\right)^2 + \left(\frac{\partial U_{Re_w}}{\partial V_{w_i}} U_{V_{w_i}}\right)^2 + \left(\frac{\partial U_{Re_w}}{\partial D_i} U_{D_i}\right)^2 + \left(\frac{\partial U_{Re_w}}{\partial \mu_{w_b}} U_{\mu_{w_b}}\right)^2},$$

where $$\frac{\partial U_{Re_w}}{\partial \rho_{w_b}} = \frac{V_{w_i}\, D_i}{\mu_{w_b}} \text{ and } U_{\rho_{w_b}} = \pm\, 0.9 \text{ kg/m}^3,$$

$$\frac{\partial U_{Re_b}}{\partial\, V_{w_i}} = \frac{\rho_{w_b}\, D_i}{\mu_{w_b}} \text{ and } U_{V_{w_i}} = \pm\, 0.001 \text{ m/s,}$$

$$\frac{\partial U_{Re_w}}{\partial D_i} = \frac{\rho_{w_b} V_{w_i}}{\mu_{w_b}} \text{ and } U_{D_i} = \pm\, 4.05\times10^{-5} \text{ m, and}$$

$$\frac{\partial U_{Re_w}}{\partial \mu_{w_b}} = -\frac{\rho_{w_b}\, V_{w_i} D_i}{\mu_{w_b}^2} \text{ and } U_{\mu_{w_b}} = \pm\, 3.1\times10^{-5} \text{ kg/m s.}$$

Thus $U_{Re_w} = \pm\, 281$ and

$$\frac{U_{Re_w}}{Re_w} = \pm\, 4.5\ \%.$$

A.20 Uncertainty Associated with the Pressure Drop Coefficient at the Air Side

The pressure drop coefficient was calculated from Eq. (4.13) as

$$P_{dc} = \frac{2\,\Delta P_a}{\rho_{a_f}\, V_{a\,max}^2}$$

For $V_{a_{max}}$ = 34.07 m/s, ρ_{a_f} = 1.177 kg/m^3, ΔP_a = 633.36 Pa and P_{dc} = 0.9272, the uncertainty in P_{dc} was calculated as follows

$$U_{P_{dc}} = \sqrt{\left(\frac{\partial P_{dc}}{\partial \Delta P_a} U_{\Delta P_a}\right)^2 + \left(\frac{\partial P_{dc}}{\partial V_{a\,max}} U_{V_{a\,max}}\right)^2 + \left(\frac{\partial P_{dc}}{\partial \rho_{a_f}} U_{\rho_{a_f}}\right)^2}\ ,$$

where $\quad \dfrac{\partial P_{dc}}{\partial \Delta P_a} = \dfrac{2}{\rho_a V_{a\,max}^2}$ and $U_{\Delta P_a} = \pm\, 5.28$ Pa,

$$\frac{\partial P_{dc}}{\partial V_{a\,max}} = -\frac{4\Delta P_a}{\rho_{a_f} V_{a\,max}^3} \text{ and } U_{V_{a\,max}} = \pm\, 0.5138 \text{ m/s, and}$$

$$\frac{\partial P_{dc}}{\partial \rho_{a_f}} = -\frac{2\Delta P_a}{\rho_{a_f}^2 V_{a\,max}^2} \text{ and } U_{\rho_{a_f}} = \pm\, 0.006 \text{ kg/m}^3.$$

Thus $\quad U_{P_{dc}} = \pm\, 0.0294$ and

$$\frac{UP_{dc}}{P_{dc}} = \pm\, 3.2\ \%.$$

VITA AUCTORIS

Mohamed Mosa was born in 1979 in Tobruk, Libya. He graduated from Assabea Menn Ebreel High School in 1996. From there he went on to Omar Al Mukhtar University at Tobruk where he obtained a B.Sc. in Mechanical Engineering in 2001. He is currently a candidate for Degree of Master of Applied Science in Mechanical Engineering at the University of Windsor.